

# On the relationship between BL Lacertae objects and radio galaxies

Hermine Landt<sup>1\*</sup> and Hayley E. Bignall<sup>2†</sup>

<sup>1</sup>*Harvard-Smithsonian Center for Astrophysics, 60 Garden Street, Cambridge, MA 02138, USA*

<sup>2</sup>*Joint Institute for VLBI in Europe, Postbus 2, NL-7990 AA Dwingeloo, The Netherlands*

Accepted . Received ; in original form

## ABSTRACT

We present deep radio images at 1.4 GHz of a large and complete sample of BL Lacertae objects (BL Lacs) selected from the Deep X-ray Radio Blazar Survey (DXRBS). We have observed 24 northern ( $\delta \gtrsim -30^\circ$ ) sources with the Very Large Array (VLA) in both its A and C configurations and 15 southern sources with the Australia Telescope Compact Array (ATCA) in its largest configuration. We find that in the DXRBS, as in the 1-Jy survey, which has a radio flux limit roughly ten times higher than the DXRBS, a considerable number (about a third) of BL Lacs can be identified with the relativistically beamed counterparts of Fanaroff-Riley type II (FR II) radio galaxies. We attribute the existence of FR II-BL Lacs, which is not accounted for by current unified schemes, to an inconsistency in our classification scheme for radio-loud active galactic nuclei (AGN). Taking the extended radio power as a suitable measure of intrinsic jet power, we find similar average values for low- (LBL) and high-energy peaked BL Lacs (HBL), contrary to the predictions of the blazar sequence.

**Key words:** BL Lacertae objects: general - galaxies: active - radio continuum: galaxies

## 1 INTRODUCTION

The basic nature of BL Lacertae objects (BL Lacs) is believed to be understood within the unified schemes for radio-loud active galactic nuclei (AGN). These sources are radio galaxies, which have their relativistic jets oriented close to the observer’s line of sight. For objects with such a preferred jet alignment, which are commonly referred to as ‘blazars’, the relativistic beaming effect can explain most of the observed properties, such as, e.g., non-thermal continuum emission from radio up to  $\gamma$ -ray frequencies, high core luminosities, core-dominated radio morphologies, irregular and rapid variability, and strong radio and optical polarization (see review by Urry & Padovani (1995) and references therein).

Current unified schemes identify the parent population of BL Lacs with the low-luminosity Fanaroff-Riley type I (FR I; Fanaroff & Riley 1974) radio galaxies, whereas the high-luminosity Fanaroff-Riley type II (FR II) radio galaxies are assumed to appear as radio quasars when their jets are viewed at relatively small angles. However, in recent years

evidence has accumulated that some BL Lacs might in fact be beamed FR II radio galaxies. Their extended radio powers are higher than those of known FR Is and their extended radio morphologies are consistent with those of FR IIs once orientation effects are accounted for (Kollgaard et al. 1992; Cassaro et al. 1999; Rector & Stocke 2001).

If indeed a considerable number of FR IIs are part of the BL Lac parent population, it will have important implications. Estimates of relativistic beaming parameters such as, e.g., the jet bulk Lorentz factor or viewing angle, which are usually derived from a comparison of the radio luminosity function (e.g., Urry et al. 1991; Urry & Padovani 1995) or the distribution of radio core-dominance values (e.g., Kollgaard et al. 1992; Perlman & Stocke 1993) of the parent population with that of the corresponding blazar class, will have to be revisited. Furthermore, since, by definition, the broad emission line region, which is assumed to trace directly the accretion disk power, is absent or only very weak in BL Lacs, the existence of a considerable number of FR II-like jet powers among this blazar class could mean that accretion disk and jet luminosities are not as closely linked as current jet formation models suggest (e.g., Blandford & Payne 1982; Rawlings & Saunders 1991; Maraschi & Tavecchio 2003).

A further implication will concern the so-called ‘blazar sequence’ (Fossati et al. 1998; Ghisellini et al. 1998). This

\* E-mail: hlandt@cfa.harvard.edu

† Current address: Curtin University of Technology, GPO Box U1987, Perth, WA 6845, Australia

model posits that Compton-cooling determines the frequency of the jet synchrotron emission peak, in particular that the higher the (intrinsic) jet power, the stronger the cooling, and the lower the synchrotron emission peak frequency. Therefore, finding in particular high-energy peaked BL Lacs with FR II-like extended radio powers could present a severe challenge for this model (see also Padovani 2007).

Our current knowledge of the radio properties of BL Lacs is based mainly on deep radio observations of two complete samples selected at widely different frequencies, namely, the radio-selected 1-Jy (Stickel et al. 1991; Rector & Stocke 2001) and the X-ray-selected *Einstein* Medium Sensitivity Survey (EMSS; Morris et al. 1991; Rector et al. 2000) BL Lac samples. However, these two surveys sample the extreme ends of the radio flux distribution of BL Lacs and, therefore, have presented a strongly biased view of BL Lac physics. In order to rectify this situation we have obtained deep radio images of a complete sample of BL Lacs with intermediate radio properties.

The paper is structured as follows. In Section 2 we discuss the selection of the BL Lac sample, for which the radio images have been obtained and analyzed as detailed in Section 3. In Section 4 we address the question of the parent population of BL Lacs. In Section 5 we investigate if some BL Lacs with featureless optical spectra are at high redshifts rather than strongly relativistically beamed. The radio properties of low- and high-energy peaked BL Lacs are compared in Section 6. Finally, Section 7 summarizes of our main results and presents our conclusions. For consistency with previous work we have assumed throughout this paper cosmological parameters  $H_0 = 50 \text{ km s}^{-1} \text{ Mpc}^{-1}$  and  $q_0 = 0$ . Energy spectral indices have been defined as  $f_\nu \propto \nu^{-\alpha}$ .

## 2 THE SAMPLE

We have selected for radio imaging BL Lacs from the Deep X-ray Radio Blazar Survey (DXRBS; Perlman et al. 1998; Landt et al. 2001; Padovani et al. 2007). In short, the DXRBS takes advantage of the fact that blazars are relatively strong X-ray and radio emitters and, by definition, have a flat radio spectrum. In this spirit it is the result of a cross-correlation between the *ROSAT* database of serendipitous X-ray sources WGACAT95 (second revision: White et al. 1995) and a number of publicly available radio catalogs (the 20 cm and 6 cm Green Bank survey catalogs NORTH20CM and GB6 (Gregory et al. 1996; White & Becker 1992) for the northern hemisphere and the 6 cm Parkes-MIT-NRAO (PMN; Griffith & Wright 1993) catalog for the southern hemisphere). All sources with radio spectral index  $\alpha_r \leq 0.7$  and off the Galactic plane ( $|b| > 10^\circ$ ) were selected as blazar candidates. Radio spectral indices for southern sources, for which a survey at a frequency different from that of the PMN was not available when the project was started, were obtained from a snapshot survey conducted with the Australia Telescope Compact Array (ATCA) at 3.6 and 6 cm.

The DXRBS complete sample is  $\sim 95$  per cent optically identified (Padovani et al. 2007). The total sample (i.e., the complete sample plus a subsample of 'low priority' sources) contains over 300 blazars, of which the large majority are

radio quasars and 44 are BL Lacs. The general properties of the DXRBS BL Lacs observed by us and with published radio data useful for our purpose are listed in Tables 1 and 2, respectively. Two DXRBS blazar candidates previously classified as BL Lacs are now considered optically unidentified based on radio images obtained as part of this program. For WGA J0023+0417, a Very Large Array (VLA) A configuration map shows the NRAO/VLA Sky Survey (NVSS) radio source, whose position was used to pinpoint the optical candidate, to be composed of two sources  $\sim 50''$  apart. For WGA J0816-0736, a VLA C array map shows a radio source with an extended core-jet morphology. The core is  $\sim 95''$  away from the observed optical candidate.

### 2.1 The Classification

The first criteria for the classification of a radio-loud AGN as a BL Lac, namely, a compact radio morphology and a completely featureless optical spectrum (Strittmatter et al. 1972), have been modified several times over the years and most recently by Landt et al. (2002, 2004). The classification problem is twofold. On the one hand, BL Lacs are blazars, i.e., they are strongly relativistically beamed, and need to be efficiently separated from radio galaxies. Following Stocke et al. (1991) and Marchã et al. (1996), this is accomplished in the DXRBS using the value of the Ca H&K break, a discontinuity in the host galaxy spectrum, which is defined as  $C = (f_+ - f_-)/f_+$ , where  $f_-$  and  $f_+$  are the fluxes in the rest-frame wavelength regions 3750–3950 Å and 4050–4250 Å, respectively. DXRBS BL Lacs are defined to have  $C < 0.4$ , since Landt et al. (2002) showed that above this value sources become increasingly lobe-dominated (see their Fig. 6).

On the other hand, blazars can have both *intrinsically* weak and strong emission line regions and a separation between BL Lacs and radio quasars is meant to reflect this. Initially, the DXRBS used the scheme proposed by Marchã et al. (1996) to classify blazars as BL Lacs. However, as discussed by Landt et al. (2004), since this scheme imposes a limit on the equivalent width of the strongest, observed emission line (i.e., narrow or broad and independent of redshift), it is rather arbitrary. Following Landt et al. (2004), the DXRBS now uses the rest-frame equivalent width plane of the narrow emission lines [O II]  $\lambda 3727$  and [O III]  $\lambda 5007$  (see their Fig. 4) to separate BL Lacs (i.e., weak-lined radio-loud AGN) and radio quasars (i.e., strong-lined radio-loud AGN). In Tables 1 and 2, column (3), we list the classification following Landt et al. (2004). For 9/44 sources we currently cannot apply their scheme since either we have no optical spectrum (4 sources) or the available spectrum does not cover the wavelength of [O III] (5 sources). We note that whereas the large majority of the DXRBS BL Lacs classified in this way are weak-lined radio-loud AGN, three sources are strong-lined radio-loud AGN, i.e., they might be more similar to radio quasars than to BL Lacs (see also Section 4.3).

### 2.2 The Redshift Determination

The weakness of both emission and absorption features in the optical spectra of BL Lacs renders the determination

**Table 1.** General Properties of the Observed Sample and Log of Observations

Object Name	CS	class	z	z type	z flag	$f_{\text{NVSS}}$ [mJy]	$\alpha_r$ (1.4-5)	$\alpha_r$ (4.8-8.6)	$f_{1\text{keV}}$ [ $\mu\text{Jy}$ ]	observation date	Array	program
(1)	(2)	(3)	(4)	(5)	(6)	(7)	(8)	(9)	(10)	(11)	(12)	(13)
WGA J0032–2849	Y	WL	0.324	abs	c	159.9	0.08	0.14	0.047	2004 Sep 30	VLA A	AL627
										2002 Sep 30	VLA C	AL578
WGA J0040–2340			0.213	?	?	52.9	0.09	0.33	0.009	2004 Oct 7	VLA A	AL627
										2002 Oct 2	VLA C	AL578
WGA J0043–2638	Y		1.003	em	c	77.8	–0.03	0.12	0.062	2004 Oct 7	VLA A	AL627
										2002 Sep 30	VLA C	AL578
WGA J0100–3337	Y		0.875	em	p	70.4	–0.42	–0.21	0.010	2004 Jan 26	ATCA 6B	C1010
WGA J0245+1047	Y	SL	0.070	em	c	417.4	0.55		0.262	2002 Feb 6	VLA A	AL564
										2005 Sep 12	VLA C	AL652
WGA J0313+4115		WL	0.029	em	c	40.6	–0.04		0.112	2002 Jan 22	VLA A	AL564
										2005 Sep 12	VLA C	AL652
WGA J0428–3805	Y	WL	0.150	abs	c	>47.9	0.58	1.98	0.004	2002 May 23	ATCA 6A	C1010
										2004 Jan 26	ATCA 6B	C1010
WGA J0431+1731	Y	WL	0.143	abs	t	374.3	0.30		0.035	2004 Jan 22	VLA A	AL564
										2002 Oct 11	VLA C	AL578
WGA J0449–4349		WL	>0.176		l			0.15	0.477	2002 May 23	ATCA 6A	C1010
										2004 Jan 26	ATCA 6B	C1010
WGA J0528–5820	Y	WL	0.254	em	c			0.70	0.031	2002 May 22	ATCA 6A	C1010
										2004 Jan 26	ATCA 6B	C1010
WGA J0533–4632	Y	WL	0.332	abs	c			0.60	0.022	2004 Jan 26	ATCA 6B	C1010
WGA J0558+5328	Y		0.036	em	c	386.4	0.59		0.040	2002 Feb 10	VLA A	AL564
										2002 Oct 11	VLA C	AL578
WGA J0624–3229	Y	WL	0.249	abs	c	42.2	–0.53		0.210	2006 Feb 6	VLA A	AP501
										2002 Oct 5	VLA C	AL578
WGA J0847+1133		WL	0.198	abs	c	32.8	0.03		3.954	2006 May 13	VLA A	AL664
										2005 Sep 12	VLA C	AL652
WGA J0940+2603	Y	WL	>0.567		l	462.2	0.05		0.082	2002 Apr 22	VLA A	AL564
										2005 Sep 12	VLA C	AL652
WGA J1204–0710	Y	WL	0.183	abs	c	167.7	0.22	0.25	0.070	2006 May 13	VLA A	AL664
										2005 Sep 12	VLA C	AL652
WGA J1231+2848		WL	>0.878		l	140.5	0.52		0.150	2002 Feb 26	VLA A	AL564
										2005 Sep 12	VLA C	AL652
WGA J1311–0521		WL	0.160	abs	c	69.8	0.36	0.23	0.040	2002 Feb 26	VLA A	AL564
										2005 Sep 12	VLA C	AL652
WGA J1320+0140			1.235	em	c	670.7	0.01		0.036	2002 Feb 4	VLA A	AL564
										2005 Sep 12	VLA C	AL652
WGA J1539–0658	Y	WL	>0.525		l	46.8	–0.27	0.47	0.018	2002 Feb 4	VLA A	AL564
										2005 Sep 12	VLA C	AL652
WGA J1744–0517	Y	WL	0.310	abs	t	196.1	0.69		0.024	2006 May 13	VLA A	AL664
										2005 Sep 12	VLA C	AL652
WGA J1808+0546	Y	WL	0.180	em	c	176.3	0.01		0.014	2006 May 13	VLA A	AL664
WGA J1834–5856	Y	WL	>0.596		l			0.00	0.102	2004 Jan 26	ATCA 6B	C1010
WGA J1834–5948	Y	WL	0.435	abs	t			0.63	0.062	2004 Jan 26	ATCA 6B	C1010
WGA J1840+5452	Y	SL	0.646	em	c	207.3	0.39		0.179	2002 Apr 7	VLA A	AL564
										2005 Sep 12	VLA C	AL652
WGA J1843–7430		WL	0.166	abs	t			0.39	0.005	2004 Jan 26	ATCA 6B	C1010
WGA J1936–4719	Y	WL	0.264	abs	p			–0.11	0.936	2004 Jan 25	ATCA 6B	C1010
WGA J2258–5525	Y	WL	0.479	em	p			0.10	0.201	2004 Jan 25	ATCA 6B	C1010
WGA J2322–4221		WL	0.089	abs	c			0.02	0.019	2004 Jan 25	ATCA 6B	C1010
WGA J2330–3724	Y	WL	0.279	em	c	304.5	0.19	–0.18	0.038	2004 Jan 25	ATCA 6B	C1010
EXO 0556–3838	Y	WL	0.302	abs	c	104.6	0.29		3.005	2002 May 22	ATCA 6A	C1010
EXO 1811+3143	Y		0.117	?	?	191.4	0.17		0.090	2002 Apr 7	VLA A	AL564
										2005 Sep 12	VLA C	AL652
MH 2136–428	Y	WL	>0.262		l			–0.13	0.113	2002 Feb 4	ATCA 6B	C1009*
PKS 2316–423		WL	0.055	em	c			0.43	0.337	2004 Jan 25	ATCA 6B	C1010
PMN J0630–24	Y	WL	1.238	abs	c	105.4	–0.16		0.322	2002 Feb 10	VLA A	AL564
										2002 Sep 20	VLA C	AL578
RX J09168+523		WL	0.190	abs	c	137.8	0.58		0.360	2002 Apr 22	VLA A	AL564
										2005 Sep 12	VLA C	AL652
TEX 0836+182	Y	WL	>0.465		l	409.9	0.17		0.080	2006 May 13	VLA A	AL664
										2002 Oct 18	VLA C	AL578

**Table 1** – *continued*

Object Name	CS	class	z	z	z	$f_{\text{NVSS}}$	$\alpha_r$	$\alpha_r$	$f_{1\text{keV}}$	observation	Array	program
(1)	(2)	(3)	(4)	type	flag	[mJy]	(1.4-5)	(4.8-8.6)	[ $\mu\text{Jy}$ ]	date	(12)	(13)
				(5)	(6)	(7)	(8)	(9)	(10)	(11)		
WGA 1012+06	Y		0.727	em	c	535.2	0.45		0.055	2006 May 13	VLA A	AL664
										2005 Sep 12	VLA C	AL652
WGA 1202+44		WL	0.297	abs	c	105.0	1.43		0.112	2006 May 13	VLA A	AL664
										2005 Sep 12	VLA C	AL652

The columns are: (1) object name; (2) 'Y' if part of the complete sample; (3) classification following Landt et al. (2004), where WL: weak-lined radio-loud AGN, SL: strong-lined radio-loud AGN; (4) redshift; (5) type of redshift, where abs: based on absorption lines, em: based on emission lines, ?: optical spectrum not published; (6) reliability of redshift, where c: certain (based on two or more lines), p: possible (based on one emission line or two or more weak absorption lines), t: tentative (based on low S/N optical spectrum), ?: optical spectrum not published, and l: lower limit estimated from the optical  $V$  magnitude following Piranomonte et al. (2007); (7) total radio flux at 1.4 GHz from the NVSS; (8) radio spectral index between 1.4 and 5 GHz, calculated from the sum of the fluxes of all NVSS sources within a  $3'$  radius (corresponding roughly to the beam size of the GB6 survey) and the total flux from the GB6 and PMN surveys for northern and southern sources, respectively; (9) radio spectral index between 4.8 and 8.6 GHz from ATCA snapshot observations; (10) unabsorbed *ROSAT* X-ray flux at 1 keV, calculated using an X-ray spectral index derived from hardness ratios; (11) observation date; (12) telescope configuration; and (13) program number.

\* observed at 4.8 GHz

**Table 2.** General Properties of the Sources with Published 1.4 GHz Observations

Object Name	CS	class	z	z	z	$f_{\text{NVSS}}$	$\alpha_r$	$f_{1\text{keV}}$	Array	Reference
(1)	(2)	(3)	(4)	type	flag	[mJy]	(1.4-5)	[ $\mu\text{Jy}$ ]	(10)	(11)
				(5)	(6)	(7)	(8)	(9)		
B2 1147+245	Y	WL	>0.292		l	797.7	-0.02	0.022	VLA A	Antonucci & Ulvestad (1985)
ON 325	Y		0.237	?	?	571.6	0.09	0.473	VLA A	Antonucci & Ulvestad (1985)
1ES 1212+078		WL	0.130	abs	c	136.6	-0.04	0.945	VLA A	Giroletti et al. (2004)
3C 66A	Y		0.444	?	?	2303.1	0.70	1.301	VLA BnA	Antonucci & Ulvestad (1985)
4C +55.17	Y	SL	0.900	em	c	3079.2	0.33	0.034	VLA A	Murphy et al. (1993)

The columns are: (1) - (8) as in Table 1; (9) unabsorbed *ROSAT* X-ray flux at 1 keV, calculated using an X-ray spectral index derived from hardness ratios; (10) telescope configuration; and (11) reference.

of their redshift a difficult task and in some cases an even impossible one. Nevertheless, based on new optical spectroscopy, which will be presented in a future paper, and a new method introduced by Piranomonte et al. (2007) all DXRBS BL Lacs now have a redshift or a lower limit thereof (Tables 1 and 2, columns (3)-(5)). Emission lines are detected in 14/40 sources, for which an optical spectrum is available. We regard the redshifts of 25/32 sources (or 78 per cent), for which an optical spectrum is available and emission and/or absorption features are detected, as firm.

The optical spectrum of 8/40 BL Lacs appears featureless. For these sources we have determined lower limits on the redshift following Piranomonte et al. (2007). Their method uses the fact that BL Lacs are hosted by ellipticals of almost constant luminosity (e.g., Urry et al. 2000), i.e., by standard candles. Then, assuming a plausible lower limit for the jet/galaxy ratio of a featureless BL Lac one can derive a lower limit on the redshift from the observed optical  $V$  magnitude.

### 3 OBSERVATIONS AND DATA REDUCTION

We have observed the northern ( $\delta \gtrsim -30^\circ$ ) sources in the sample (24 objects) with the VLA and the southern sources (15 objects) with the ATCA. In Table 1 we give the log of our observations. Another five northern sources have published radio data useful for our purpose and were not reobserved. These are listed in Table 2 with the corresponding references.

The VLA observations were conducted in continuum mode whereby two channels of 50 MHz bandwidth were centered at 1.385 and 1.465 GHz, resulting in an effective frequency of 1.425 GHz. During a period of several years, between January 2002 and May 2006, we imaged all sources with both the VLA A and C configurations. The only exception was the source WGA J1808+0546, which we imaged only with the VLA A array. Typically three or four scans of several minutes length spaced to optimize the  $(u, v)$  plane coverage were interleaved with one minute scans on a suitable secondary VLA calibrator for each source. This yielded total source exposure times of  $\sim 30 - 45$  minutes, corresponding to a theoretical rms sensitivity of  $\sim 0.05$  mJy/beam. Multiple observations of 3C 48, 3C 147, or 3C 286 were used to flux-calibrate the maps.

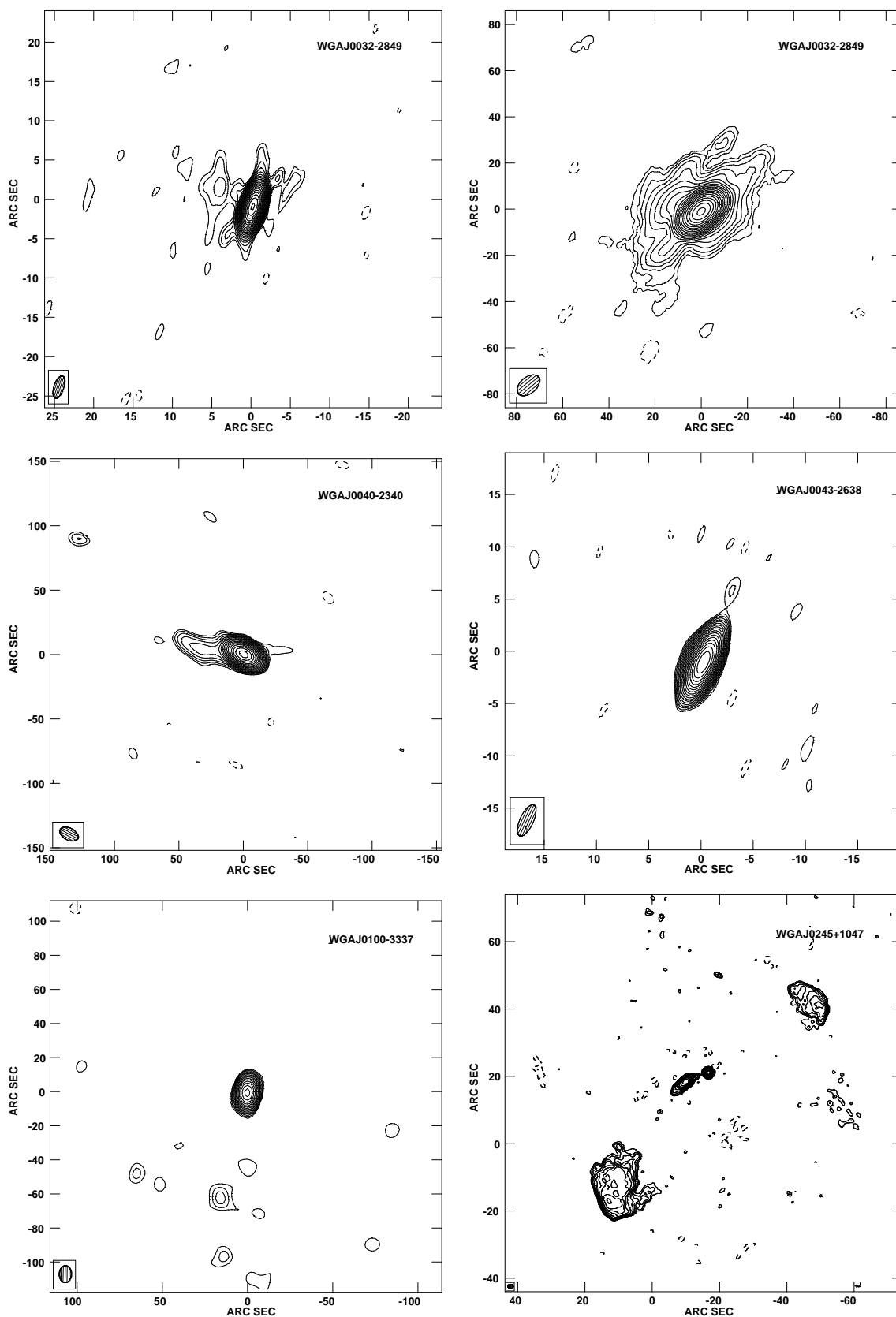


**Figure 1.** (a) WGA J0032–2849, VLA A. Image rms is 0.07 mJy/beam. Image peak is 151.8 mJy/beam. (b) WGA J0032–2849, VLA A+C. Image rms is 0.06 mJy/beam. Image peak is 144.6 mJy/beam. (c) WGA J0040–2340, VLA C. Image rms is 0.05 mJy/beam. Image peak is 45.9 mJy/beam. (d) WGA J0043–2638, VLA A. Image rms is 0.05 mJy/beam. Image peak is 76.4 mJy/beam. (e) WGA J0100–3337, ATCA 6B. Image rms is 0.20 mJy/beam. Image peak is 90.1 mJy/beam. (f) WGA J0245+1047, VLA A. Image rms is 0.04 mJy/beam. Image peak is 28.6 mJy/beam. In all images contours start at 3 times the rms and positive values are spaced by factors of  $\sqrt{2}$ .

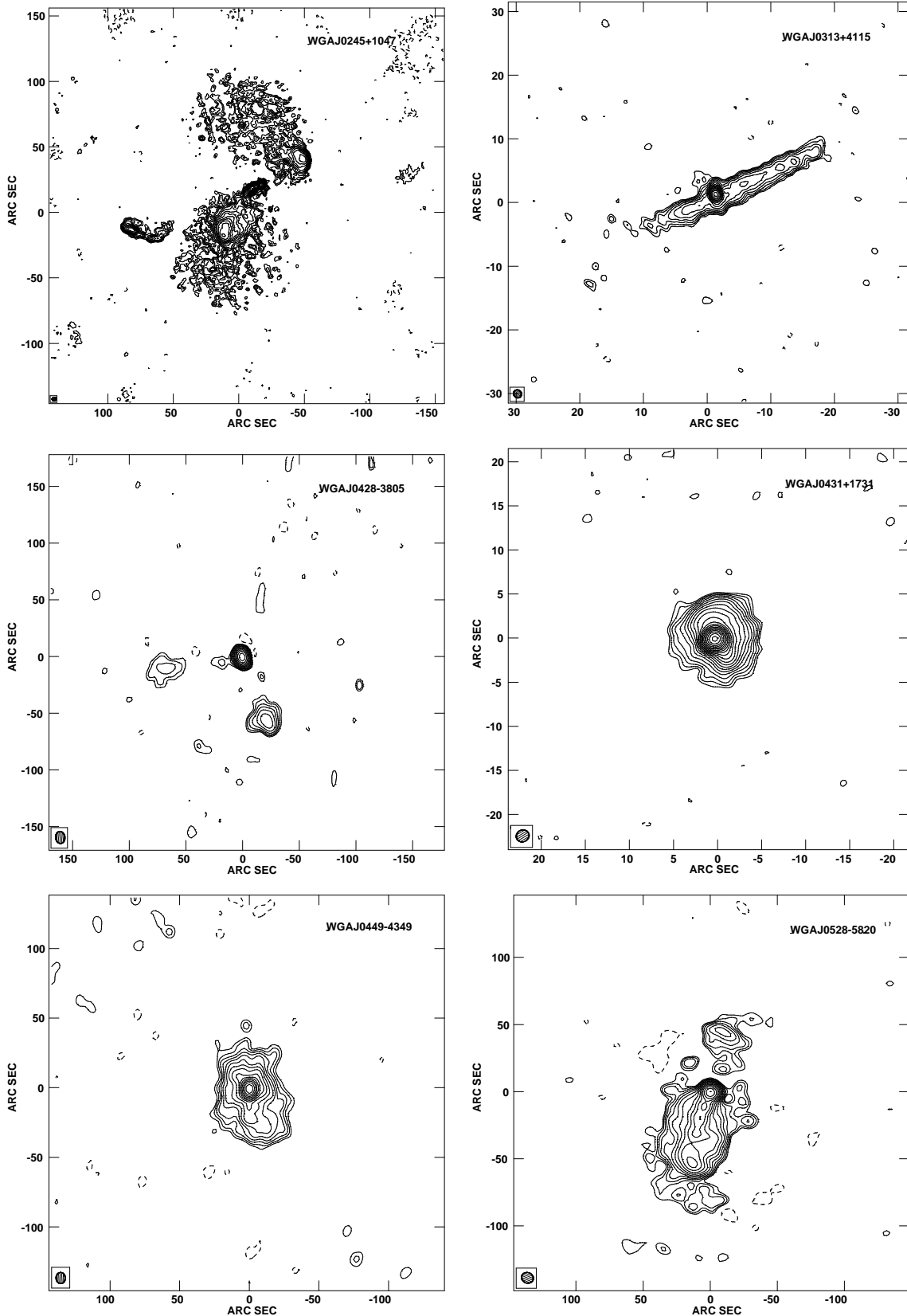


**Figure 2.** (a) WGA J0245+1047, VLA A+C. Image rms is 0.04 mJy/beam. Image peak is 30.5 mJy/beam. (b) WGA J0313+4115, VLA A. Image rms is 0.17 mJy/beam. Image peak is 54.8 mJy/beam. (c) WGA J0428-3805, ATCA 6A+6B. Image rms is 0.24 mJy/beam. Image peak is 476.5 mJy/beam. (d) WGA J0431+1731, VLA A. Image rms is 0.08 mJy/beam. Image peak is 262.6 mJy/beam. (e) WGA J0449-4349, ATCA 6A+6B. Image rms is 0.18 mJy/beam. Image peak is 99.3 mJy/beam. (f) WGA J0528-5820, ATCA 6A+6B. Image rms is 0.10 mJy/beam. Image peak is 26.1 mJy/beam. Contours and positive values as in Fig. 1.

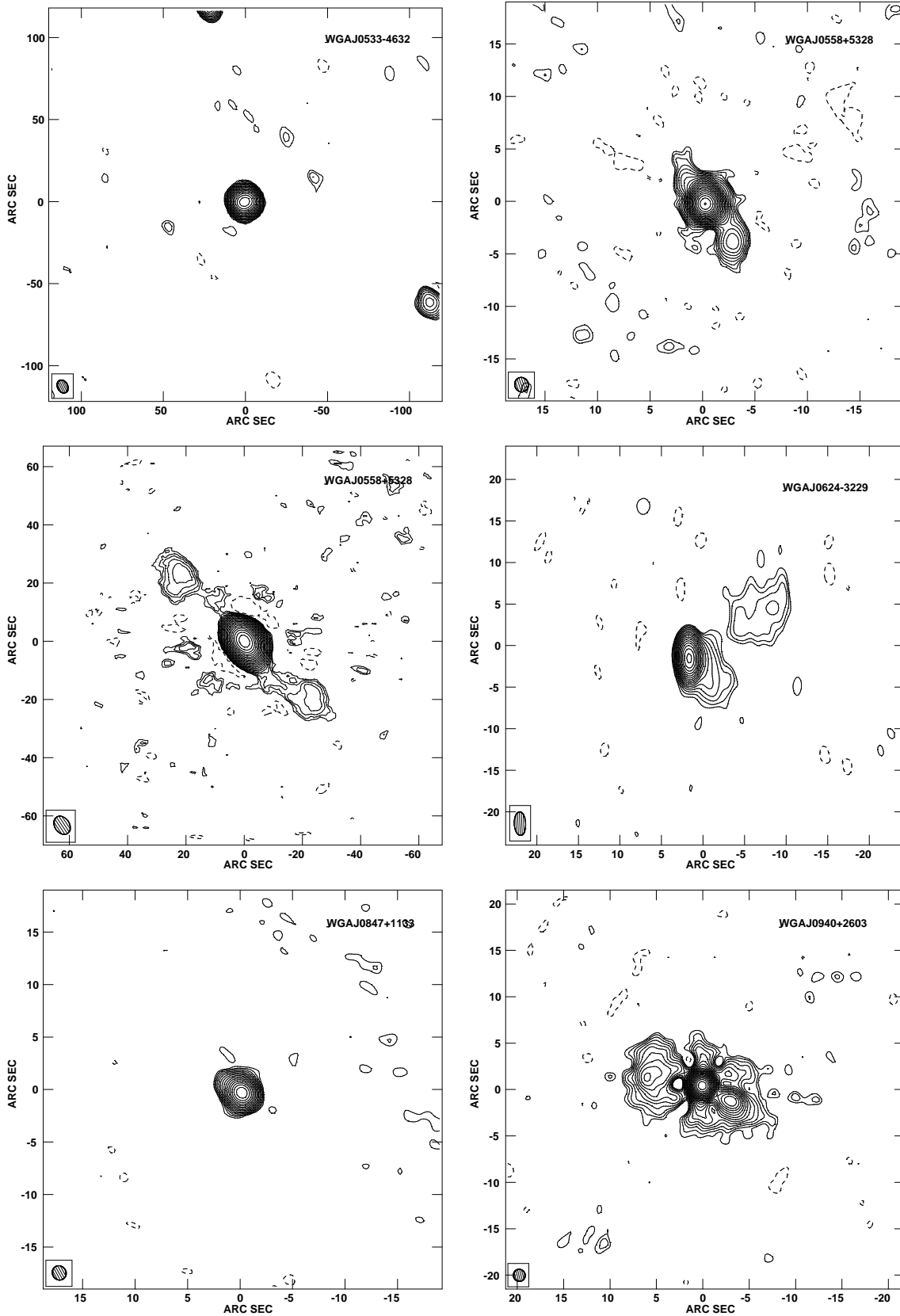


**Figure 3.** (a) WGA J0533-4632, ATCA 6B. Image rms is 0.11 mJy/beam. Image peak is 108.2 mJy/beam. (b) WGA J0558+5328, VLA A. Image rms is 0.07 mJy/beam. Image peak is 296.9 mJy/beam. (c) WGA J0558+5328, VLA A+C. Image rms is 0.06 mJy/beam. Image peak is 355.1 mJy/beam. (d) WGA J0624-3229, VLA A. Image rms is 0.06 mJy/beam. Image peak is 34.8 mJy/beam. (e) WGA J0847+1133, VLA A. Image rms is 0.05 mJy/beam. Image peak is 26.9 mJy/beam. (f) WGA J0940+2603, VLA A. Image rms is 0.06 mJy/beam. Image peak is 371.7 mJy/beam. Contours and positive values as in Fig. 1.

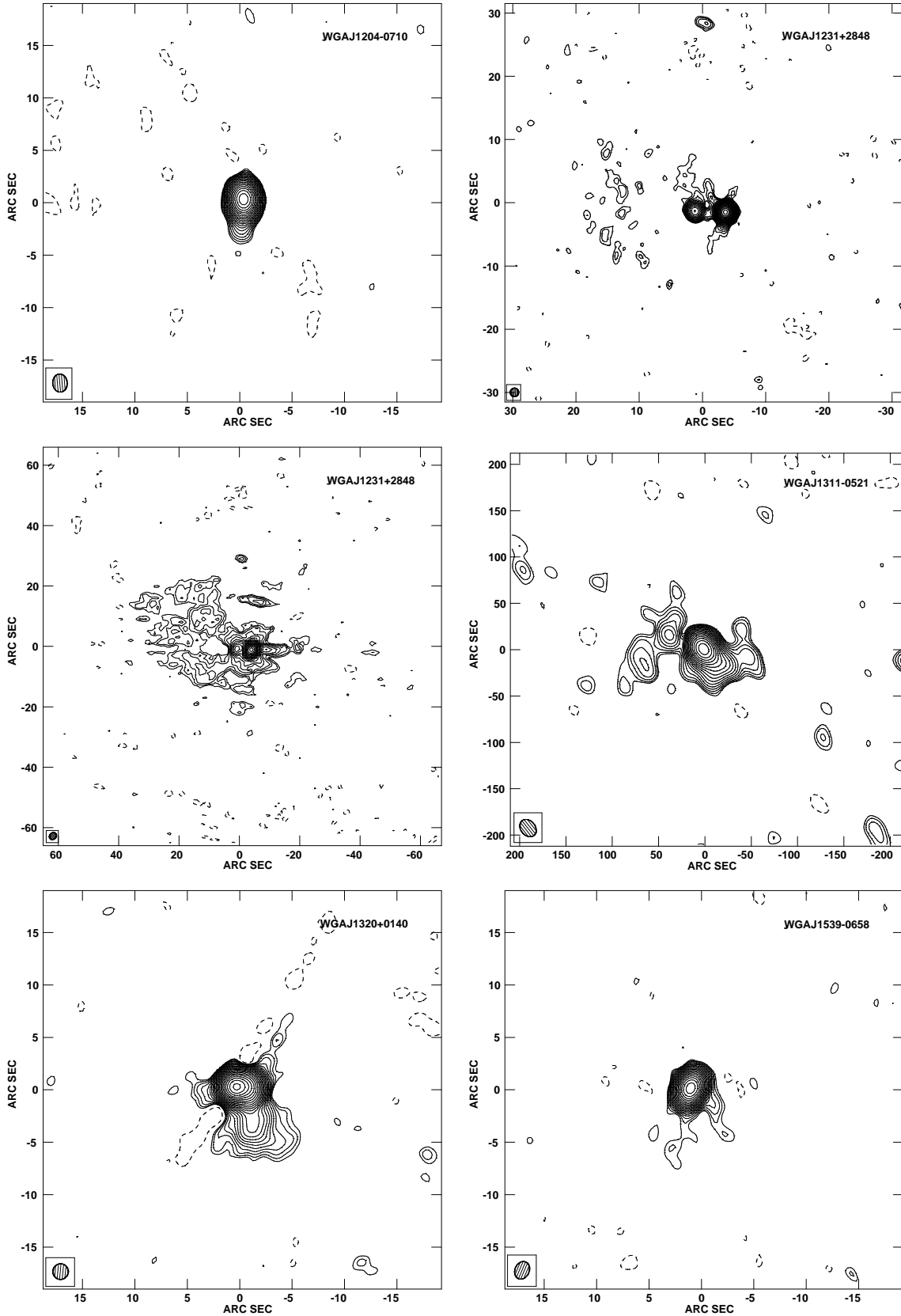


**Figure 4.** (a) WGA J1204–0710, VLA A. Image rms is 0.08 mJy/beam. Image peak is 148.1 mJy/beam. (b) WGA J1231+2848, VLA A. Image rms is 0.02 mJy/beam. Image peak is 85.6 mJy/beam. (c) WGA J1231+2848, VLA A+C. Image rms is 0.04 mJy/beam. Image peak is 90.5 mJy/beam. (d) WGA J1311–0521, VLA C. Image rms is 0.07 mJy/beam. Image peak is 79.1 mJy/beam. (e) WGA J1320+0140, VLA A. Image rms is 0.07 mJy/beam. Image peak is 496.5 mJy/beam. (f) WGA J1539–0658, VLA A. Image rms is 0.02 mJy/beam. Image peak is 43.5 mJy/beam. Contours and positive values as in Fig. 1.

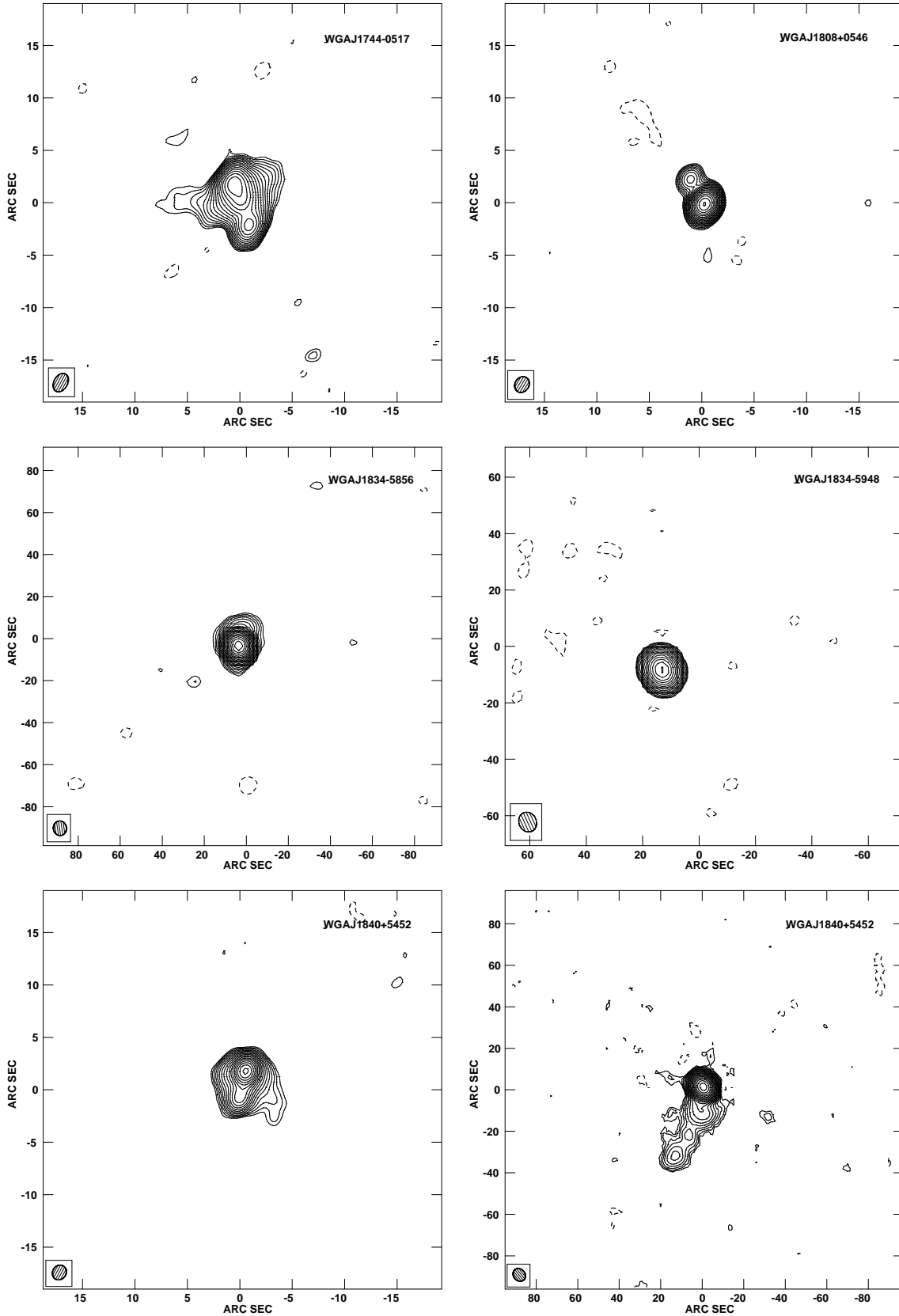


**Figure 5.** (a) WGA J1744-0517, VLA A. Image rms is 0.12 mJy/beam. Image peak is 62.6 mJy/beam. (b) WGA J1808+0546, VLA A. Image rms is 0.19 mJy/beam. Image peak is 215.3 mJy/beam. (c) WGA J1834-5856, ATCA 6B. Image rms is 0.12 mJy/beam. Image peak is 351.7 mJy/beam. (d) WGA J1834-5948, ATCA 6B. Image rms is 0.22 mJy/beam. Image peak is 170.7 mJy/beam. (e) WGA J1840+5452, VLA A. Image rms is 0.12 mJy/beam. Image peak is 101.9 mJy/beam. (f) WGA J1840+5452, VLA A+C. Image rms is 0.11 mJy/beam. Image peak is 139.9 mJy/beam. Contours and positive values as in Fig. 1.

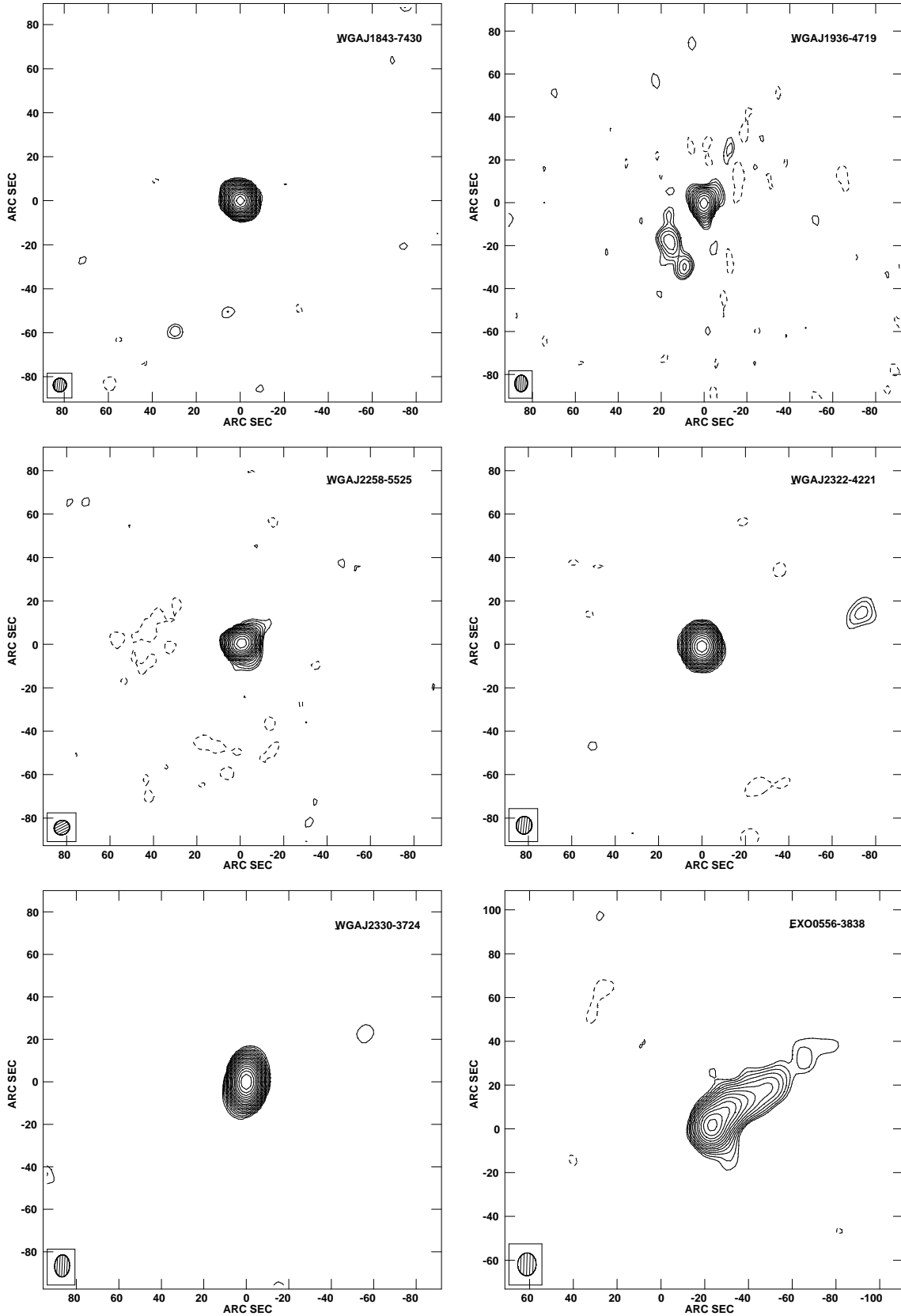


**Figure 6.** (a) WGA J1843–7430, ATCA 6B. Image rms is 0.07 mJy/beam. Image peak is 71.0 mJy/beam. (b) WGA J1936–4719, ATCA 6B. Image rms is 0.39 mJy/beam. Image peak is 98.7 mJy/beam. (c) WGA J2258–5525, ATCA 6B. Image rms is 0.13 mJy/beam. Image peak is 65.4 mJy/beam. (d) WGA J2322–4221, ATCA 6B. Image rms is 0.10 mJy/beam. Image peak is 69.2 mJy/beam. (e) WGA J2330–3724, ATCA 6B. Image rms is 0.23 mJy/beam. Image peak is 345.2 mJy/beam. (f) EXO 0556–3838, ATCA 6A. Image rms is 0.20 mJy/beam. Image peak is 43.3 mJy/beam. Contours and positive values as in Fig. 1.

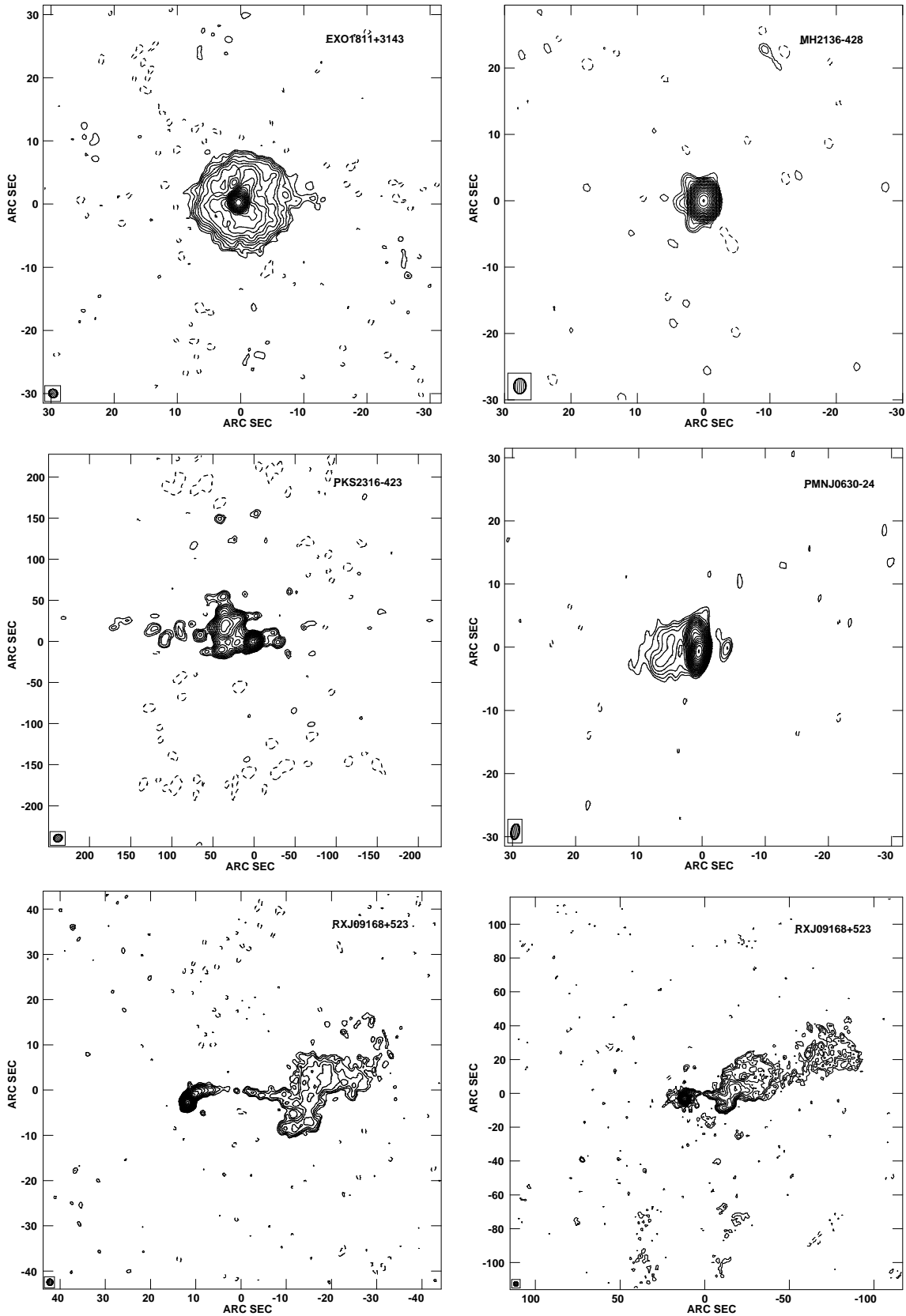


**Figure 7.** (a) EXO 1811+3143, VLA A. Image rms is 0.02 mJy/beam. Image peak is 102.8 mJy/beam. (b) MH 2136–428, ATCA 6B at 4.8 GHz. Image rms is 0.04 mJy/beam. Image peak is 62.1 mJy/beam. (c) PKS 2316–423, ATCA 6B. Image rms is 0.40 mJy/beam. Image peak is 247.5 mJy/beam. (d) PMN J0630–24, VLA A. Image rms is 0.04 mJy/beam. Image peak is 87.1 mJy/beam. (e) RX J09168+523, VLA A. Image rms is 0.02 mJy/beam. Image peak is 57.8 mJy/beam. (f) RX J09168+523, VLA A+C. Image rms is 0.04 mJy/beam. Image peak is 61.1 mJy/beam. Contours and positive values as in Fig. 1.

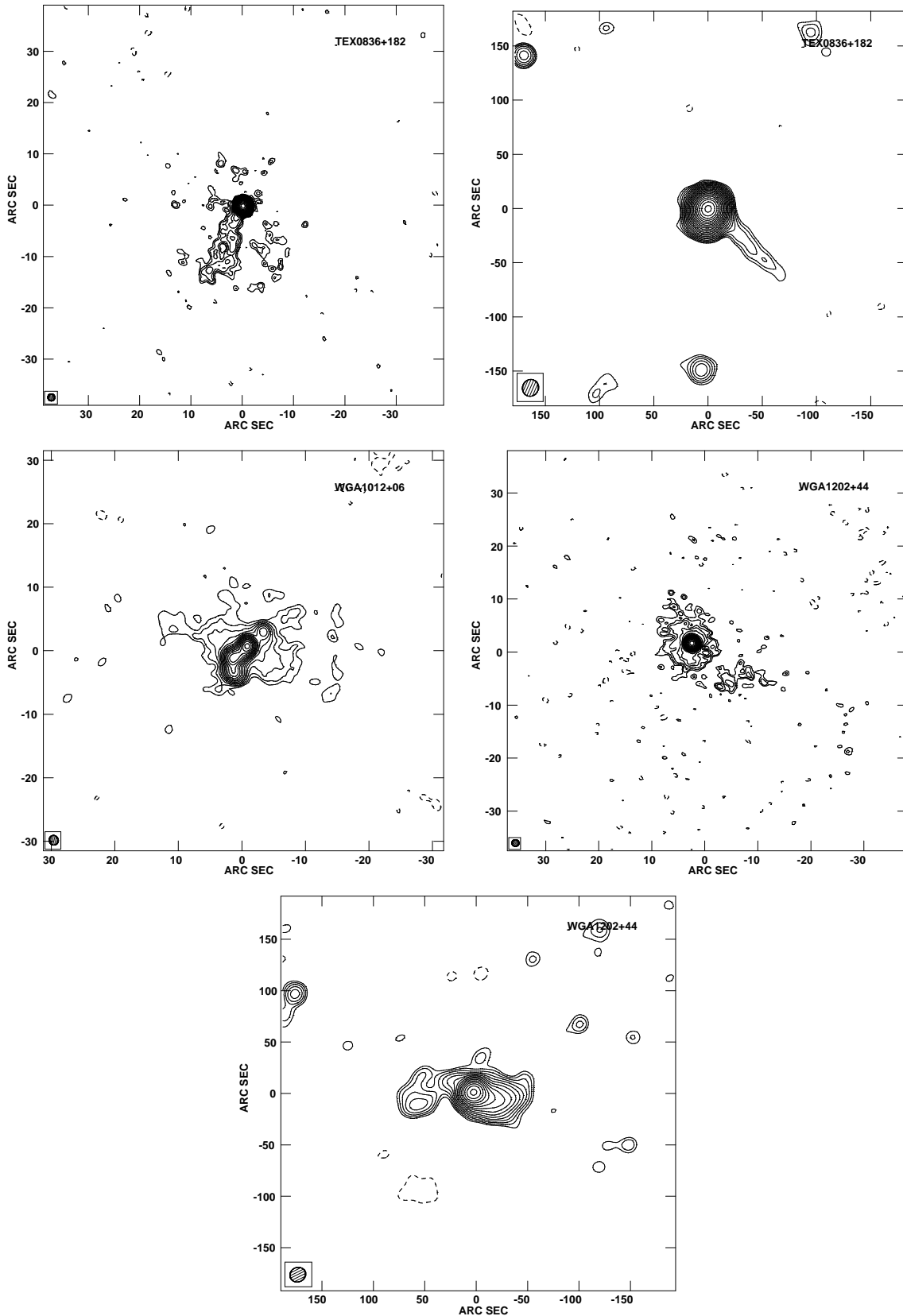


**Figure 8.** (a) TEX 0836+182, VLA A. Image rms is 0.08 mJy/beam. Image peak is 308.3 mJy/beam. (b) TEX 0836+182, VLA C. Image rms is 0.11 mJy/beam. Image peak is 363.5 mJy/beam. (c) WGA 1012+06, VLA A. Image rms is 0.36 mJy/beam. Image peak is 166.4 mJy/beam. (d) WGA 1202+44, VLA A. Image rms is 0.03 mJy/beam. Image peak is 48.5 mJy/beam. (e) WGA 1202+44, VLA C. Image rms is 0.14 mJy/beam. Image peak is 81.9 mJy/beam. Contours and positive values as in Fig. 1.

Table 3. Map Parameters

Object Name	Array	Beam [arcsec]	PA [deg]	rms [mJy/ beam]	Peak [mJy/ beam]	Scale [kpc/ arcsec]	Figure
(1)	(2)	(3)	(4)	(5)	(6)	(7)	(8)
WGA J0032–2849	VLA A	3.0× 1.3	–18	0.07	151.8	6.2	1a
WGA J0032–2849	VLA A+C	11.3× 7.0	–50	0.06	144.6	6.2	1b
WGA J0040–2340	VLA C	15.2× 9.3	62	0.05	45.9	4.7	1c
WGA J0043–2638	VLA A	3.3× 1.3	–25	0.05	76.4	10.9	1d
WGA J0100–3337	ATCA 6B	10.0× 7.1	–1	0.20	90.1	10.4	1e
WGA J0245+1047	VLA A	1.4× 1.4	75	0.04	28.6	1.8	1f
WGA J0245+1047	VLA A+C	3.0× 2.6	–66	0.04	30.5	1.8	2a
WGA J0313+4115	VLA A	1.3× 1.2	28	0.17	54.8	0.8	2b
WGA J0428–3805	ATCA 6A+6B	10.7× 8.0	6	0.24	476.5	3.5	2c
WGA J0431+1731	VLA A	1.5× 1.3	–59	0.08	262.6	3.4	2d
WGA J0449–4349	ATCA 6A+6B	8.0× 6.5	3	0.18	99.3	>4.0	2e
WGA J0528–5820	ATCA 6A+6B	8.9× 7.9	66	0.10	26.1	5.3	2f
WGA J0533–4632	ATCA 6B	8.3× 6.1	26	0.11	108.2	6.3	3a
WGA J0558+5328	VLA A	1.4× 1.3	19	0.07	296.9	1.0	3b
WGA J0558+5328	VLA A+C	6.8× 5.1	33	0.06	355.1	1.0	3c
WGA J0624–3229	VLA A	2.8× 1.4	3	0.06	34.8	5.2	3d
WGA J0847+1133	VLA A	1.4× 1.3	28	0.05	26.9	4.4	3e
WGA J0940+2603	VLA A	1.3× 1.2	15	0.06	371.7	>8.6	3f
WGA J1204–0710	VLA A	1.7× 1.4	5	0.08	148.1	4.1	4a
WGA J1231+2848	VLA A	1.4× 1.3	–3	0.02	85.6	>10.4	4b
WGA J1231+2848	VLA A+C	2.5× 2.1	–38	0.04	90.5	>10.4	4c
WGA J1311–0521	VLA C	20.4× 15.7	38	0.07	79.1	3.7	4d
WGA J1320+0140	VLA A	1.5× 1.5	–5	0.07	496.5	11.6	4e
WGA J1539–0658	VLA A	1.7× 1.4	–23	0.02	43.5	>8.3	4f
WGA J1744–0517	VLA A	1.9× 1.3	–28	0.12	62.6	6.1	5a
WGA J1808+0546	VLA A	1.6× 1.3	–31	0.19	215.3	4.1	5b
WGA J1834–5856	ATCA 6B	7.0× 6.2	8	0.12	351.7	>8.8	5c
WGA J1834–5948	ATCA 6B	7.2× 6.2	24	0.22	170.7	7.5	5d
WGA J1840+5452	VLA A	1.5× 1.3	–29	0.12	101.9	9.2	5e
WGA J1840+5452	VLA A+C	6.6× 5.5	38	0.11	139.9	9.2	5f
WGA J1843–7430	ATCA 6B	6.3× 5.9	–6	0.07	71.0	3.8	6a
WGA J1936–4719	ATCA 6B	7.7× 5.8	–2	0.39	98.7	5.4	6b
WGA J2258–5525	ATCA 6B	7.2× 6.6	–63	0.13	65.4	7.9	6c
WGA J2322–4221	ATCA 6B	8.2× 7.1	–7	0.10	69.2	2.3	6d
WGA J2330–3724	ATCA 6B	10.4× 7.0	–3	0.23	345.2	5.6	6e
EXO 0556–3838	ATCA 6A	10.4× 8.4	–2	0.20	43.3	6.0	6f
EXO 1811+3143	VLA A	1.4× 1.3	42	0.02	102.8	2.9	7a
MH 2136–428*	ATCA 6B	2.3× 1.8	–3	0.04	62.1	>5.4	7b
PKS 2316–423	ATCA 6B	10.1× 8.8	–60	0.40	247.5	1.5	7c
PMN J0630–24	VLA A	2.5× 1.3	–10	0.04	87.1	11.6	7d
RX J09168+523	VLA A	1.4× 1.2	2	0.02	57.8	4.3	7e
RX J09168+523	VLA A+C	2.6× 2.3	14	0.04	61.1	4.3	7f
TEX 0836+182	VLA A	1.4× 1.3	6	0.08	308.3	>7.8	8a
TEX 0836+182	VLA C	15.8× 14.5	–24	0.11	363.5	>7.8	8b
WGA 1012+06	VLA A	1.5× 1.4	13	0.36	166.4	9.7	8c
WGA 1202+44	VLA A	1.3× 1.3	52	0.03	48.5	5.9	8d
WGA 1202+44	VLA C	15.5× 14.0	–63	0.14	81.9	5.9	8e

The columns are: (1) object name; (2) telescope configuration; (3) beam size; (4) position angle; (5) image rms; (6) peak flux; (7) physical scale in the object’s rest-frame; and (8) corresponding panel in Figs. 1-8.

\* observed at 4.8 GHz

The VLA data were processed with the Astronomical Image Processing System (AIPS; version 31DEC06) package. A model based on Clean components was used to start the self-calibration process. Phase-only self-calibration was used for the first three iterations and amplitude and phase self-calibration for the last one or two iterations. The task

IMAGR with robust weighting (ROBUST=0.5) was used to generate the maps and Clean components. We found it useful to combine the self-calibrated data sets from the A and C arrays in order to increase the sensitivity and to improve the  $(u, v)$  plane coverage in only 6/23 cases.

The ATCA continuum observations were performed

with a bandwidth of 128 MHz centered at 1.384 GHz. The observations were carried out in two 13 hour sessions in May 2002 in the 6A configuration and in a single session of 32 hours in January 2004 in the 6B configuration. Typically sources were observed in scans of  $\sim 10 - 15$  minutes spread over a wide range of hour angles, interleaved with two minute scans on a nearby secondary calibrator. The total integration time on each source ranged between  $\sim 2 - 5$  hours, resulting in theoretical rms sensitivity of  $\sim 0.05$  mJy/beam. The rms noise in the final images was a factor of two or more larger than this due to the presence of confusing sources in the primary beam. The source MH 2136–428 was included in a different program and was observed instead at 4.8 GHz. The ATCA data reduction was performed using standard procedures in the MIRIAD software package. The images were produced in either MIRIAD or Difmap using a similar method to that used for the VLA data. The flux density scale is tied to the ATCA primary calibrator PKS 1934–638.

The final maps are shown in Figs. 1 - 8 and the corresponding map parameters are listed in Table 3. The dynamic ranges (peak/noise) of the VLA maps lie between  $\sim 300 - 7000$  and those of the ATCA maps between  $\sim 200 - 3000$ , with typical values of  $\sim 2000$  and  $1000$ , respectively. In Table 4 we list the radio properties of the sources as derived from our observations using the AIPS task TVSTAT. The core flux density was measured as the peak of the core emission on the VLA A array map and (combined) ATCA map for the northern and southern sources, respectively. The extended flux density was derived by subtracting the core flux density from the total flux density, the latter measured on the VLA C array map, if the source was resolved, else measured on the VLA A array map, for the northern sources, and on the (combined) ATCA map for the southern sources. We give  $1\sigma$  cumulative errors for the extended flux densities, which depend upon the solid angular extent of the measured flux.

We have detected extended radio emission for all sources observed with the VLA, with the exception of WGA J0043–2638. For about half of these objects (13/24 sources) the extended emission is visible only on the small scales typical of the A array and the source remains unresolved on the C array map. Similarly, 6/15 sources (or 40 per cent) observed with the ATCA remain unresolved on the scales imaged. Since the angular resolution of the ATCA is intermediate between that of the VLA A and C array, the non-detection of extended radio emission in these sources is most likely due to resolution rather than to sensitivity. Therefore, we have derived upper limits on the extended radio emission for the seven unresolved sources in our sample by assuming the most basic definition of a blazar, i.e., a radio core-dominance parameter  $R = L_{\text{core}}/L_{\text{ext}} > 1$ , where  $L_{\text{core}}$  and  $L_{\text{ext}}$  are the radio core and extended luminosities, respectively. For these sources the core flux densities listed in Table 4, column (5), are then assumed to be the *total* flux densities.

#### 4 THE PARENT POPULATION

Current unified schemes for radio-loud AGN posit that BL Lacs are the relativistically beamed counterparts of the low-luminosity FR I radio galaxies, i.e., that they are FR

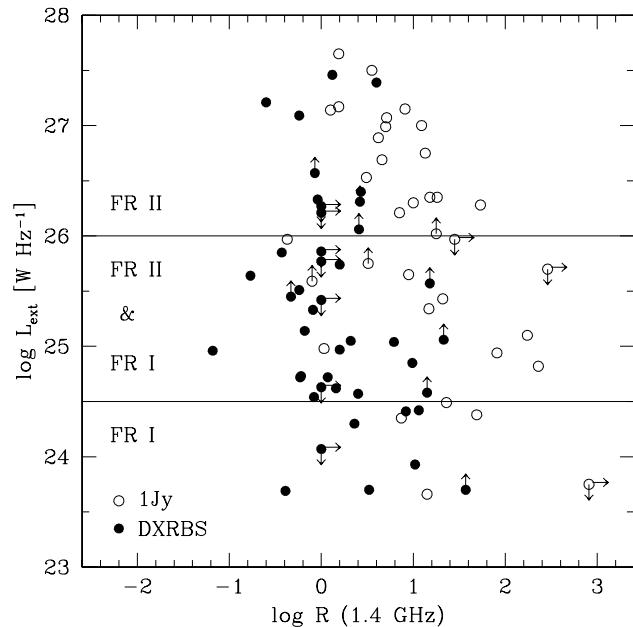


**Figure 9.** The extended radio power versus the radio core dominance parameter  $R$  at 1.4 GHz, where  $R = L_{\text{core}}/L_{\text{ext}}$ , with  $L_{\text{core}}$  and  $L_{\text{ext}}$  the radio core and extended luminosities, respectively. Open and filled circles indicate BL Lacs from the 1Jy survey and the DXRBS, respectively. Arrows indicate limits. The horizontal solid lines mark the regions of extended radio powers typical of FR I and FR II radio galaxies.

Is with their radio jets aligned close to our line of sight (Urry & Padovani 1995, and references therein). Since at small viewing angles orientation and projection effects make the recognition of the FR class of the extended radio morphology difficult, this unification scheme relies mainly on comparisons between the extended radio powers of FR Is and BL Lacs, which, believed to be isotropic and therefore unaffected by relativistic beaming, are expected to be similar.

Nevertheless, as high-quality radio imaging campaigns have shown, the connection between BL Lacs and radio galaxies seems to be more complicated. BL Lacs with high, FR II-like extended radio powers appear to be present in considerable numbers in surveys with relatively high radio flux limits, such as, e.g., the 1-Jy survey (Kollgaard et al. 1992; Murphy et al. 1993; Cassaro et al. 1999; Rector & Stocke 2001). In this section we show that also in the DXRBS, a survey with a roughly ten times lower radio flux limit than the 1-Jy survey, numerous BL Lacs can be associated with relativistically beamed FR IIs (Sections 4.1 and 4.2). As we discuss in Section 4.3, the existence of FR II BL Lacs is in fact *expected* considering the current classification scheme for radio-loud AGN and calls for a revision of the unified schemes.

##### 4.1 The Distribution of Extended Radio Powers

In Fig. 9 we have plotted for the DXRBS BL Lac sample (filled circles) the radio core-dominance parameter  $R$  versus the extended radio luminosity at 1.4 GHz. The figure shows

**Table 4.** Observed 1.4 GHz Radio Properties of the Sample

Object Name	Array	R.A.(J2000)	Decl.(J2000)	$f_{\text{core}}$ [mJy]	$f_{\text{ext}}$ [mJy]	$\log L_{\text{core}}$ [W/Hz]	$\log L_{\text{ext}}$ [W/Hz]	$\log R$	LAS [arcsec]	$\log(L_{\text{core}}/L_{\text{x}})$
(1)	(2)	(3)	(4)	(5)	(6)	(7)	(8)	(9)	(10)	(11)
WGA J0032–2849	VLA	00 32 33.081	–28 49 20.00	151.8	12.2±0.3	25.84	24.85	0.99	34.6	6.36
WGA J0040–2340	VLA	00 40 24.892	–23 40 00.80	45.7	3.7±0.2	24.95	23.93	1.02	18.4	6.60
WGA J0043–2638	VLA	00 43 22.731	–26 39 06.10	76.4	...	26.57	<26.27	>0.00	<3.3	5.73
WGA J0100–3337	ATCA	01 00 09.400	–33 37 31.00	90.1	...	26.51	<26.21	>0.00	<10.0	6.62
WGA J0245+1047	VLA	02 45 13.473	+10 47 22.70	28.6	408.7±0.9	23.78	24.96	–1.18	104.1	5.00
WGA J0313+4115	VLA	03 13 57.649	+41 15 23.85	54.8	133.0±1.9	23.30	23.69	–0.39	14.2	5.68
WGA J0428–3805	ATCA	04 28 50.800	–38 05 50.00	29.7	32.1±2.1	24.46	24.54	–0.08	68.1	6.80
WGA J0431+1731	VLA	04 31 57.367	+17 31 35.90	262.6	113.1±0.5	25.37	25.05	0.32	2.8	6.81
WGA J0449–4349	ATCA	04 49 24.700	–43 50 08.00	99.3	183.2±1.9	>25.12	>25.45	–0.33	16.8	5.23
WGA J0528–5820	ATCA	05 28 34.699	–58 20 17.99	26.1	128.2±1.3	24.87	25.64	–0.77	54.2	5.81
WGA J0533–4632	ATCA	05 33 40.799	–46 32 15.00	108.2	...	25.72	<25.42	>0.00	<8.3	6.54
WGA J0558+5328	VLA	05 58 11.822	+53 28 17.75	296.9	88.0±0.3	24.22	23.70	0.52	31.5	6.85
WGA J0624–3229	VLA	06 24 45.058	–32 30 54.85	34.8	11.4±0.4	24.97	24.57	0.40	11.8	5.10
WGA J0847+1133	VLA	08 47 12.940	+11 33 50.25	26.9	10.2±0.2	24.66	24.30	0.36	1.5	3.74
WGA J0940+2603	VLA	09 40 14.720	+26 03 30.00	371.7	97.3±0.5	>26.73	>26.31	0.42	6.0	6.42
WGA J1204–0710	VLA	12 04 16.656	–07 10 09.25	148.1	15.5±0.3	25.33	24.41	0.92	3.0	6.24
WGA J1231+2848	VLA	12 31 43.565	+28 47 49.70	85.6	61.6±0.7	>26.50	>26.57	–0.07	24.0	5.43
WGA J1311–0521	VLA	13 11 17.840	–05 21 20.00	27.7	42.2±0.4	24.49	24.72	–0.23	94.8	5.77
WGA J1320+0140	VLA	13 20 26.787	+01 40 36.75	496.5	198.6±0.3	27.58	27.46	0.12	3.6	6.72
WGA J1539–0658	VLA	15 39 09.677	–06 58 43.15	43.5	2.2±0.2	>25.73	>24.58	1.15	6.0	6.16
WGA J1744–0517	VLA	17 44 20.883	–05 18 39.55	62.6	135.8±0.7	25.42	25.85	–0.43	4.2	6.27
WGA J1808+0546	VLA	18 08 32.223	+05 46 51.85	215.3	16.4±0.7	25.48	24.42	1.06	2.8	7.10
WGA J1834–5856	ATCA	18 34 27.479	–58 56 36.71	351.7	16.0±0.6	>26.75	>25.57	1.18	9.3	6.29
WGA J1834–5948	ATCA	18 34 15.324	–59 48 46.43	170.7	...	26.16	<25.86	>0.00	<7.2	6.25
WGA J1840+5452	VLA	18 40 57.382	+54 52 15.85	101.9	75.2±0.3	26.29	26.33	–0.04	29.7	5.50
WGA J1843–7430	ATCA	18 43 40.198	–74 30 24.99	71.0	...	24.93	<24.63	>0.00	<6.3	7.07
WGA J1936–4719	ATCA	19 36 56.100	–47 19 50.00	49.2	25.4±2.1	25.17	24.97	0.20	30.5	4.59
WGA J2258–5525	ATCA	22 58 19.098	–55 25 37.99	65.4	7.9±0.5	25.83	25.04	0.79	9.5	5.31
WGA J2322–4221	ATCA	23 22 40.398	–42 20 43.89	69.2	...	24.37	<24.07	>0.00	<8.2	6.51
WGA J2330–3724	ATCA	23 30 35.798	–37 24 37.00	345.2	...	26.07	<25.77	>0.00	<10.4	6.83
B2 1147+245	VLA	11 50 19.22	+24 17 53.7	664	25	>26.39	>25.06	1.33	26.6	7.34
EXO 0556–3838	ATCA	05 58 06.477	–38 38 31.12	43.3	43.0±1.1	25.24	25.33	–0.09	22.9	4.02
EXO 1811+3143	VLA	18 13 35.190	+31 44 17.65	102.8	64.0±0.3	24.78	24.62	0.16	3.8	6.00
MH 2136–428*	ATCA	21 39 24.140	–42 35 21.30	62.1	1.4±0.2	>25.27	>23.70	1.57	2.5	5.62
ON 325	VLA	12 17 52.11	+30 07 00.0	355	189	25.94	25.74	0.20	95.0	5.77
PKS 2316–423	ATCA	23 19 05.963	–42 06 49.00	247.5	391.9±4.9	24.51	24.73	–0.22	169.8	5.84
PMN J0630–24	VLA	06 30 59.527	–24 06 46.05	87.1	16.9±0.3	26.83	26.40	0.43	6.5	5.01
RX J09168+523	VLA	09 16 51.921	+52 38 28.45	57.8	77.6±0.4	24.96	25.14	–0.18	95.6	5.12
TEX 0836+182	VLA	08 39 30.712	+18 02 47.05	308.3	88.3±0.5	>26.47	>26.06	0.41	90.3	6.38
WGA 1012+06	VLA	10 12 13.360	+06 30 57.05	166.4	424.1±3.6	26.61	27.21	–0.60	8.8	6.20
WGA 1202+44	VLA	12 02 08.665	+44 44 22.55	48.5	67.4±1.0	25.27	25.51	–0.24	57.2	5.50
1ES 1212+078	VLA	12 15 10.88	+07 32 05.2	85	65	24.79	24.72	0.07		4.89
3C 66A	VLA	02 22 39.48	+43 02 08.4	814	1052	26.85	27.09	–0.24	43.4	5.60
4C +55.17	VLA	09 57 38.18	+55 22 57.4	2568	381	28.00	27.39	0.60	3.1	7.55

The columns are: (1) object name; (2) telescope used for observations; (3) and (4) position of the unresolved core, measured on VLA A array or (combined) ATCA map (NVSS position is given for sources listed in Table 2); (5) core flux density, measured on VLA A array or (combined) ATCA map; (6) extended flux density, derived from the total flux density measured on VLA C array map (if the source was resolved, else measured on VLA A array map) or (combined) ATCA map subtracting the core flux density given in column (5); (7) core luminosity  $k$ -corrected with spectral index  $\alpha_r = 0$ ; (8) extended luminosity  $k$ -corrected with spectral index  $\alpha_r = 0.8$ ; (9) radio core-dominance parameter  $R$ , defined as  $R = L_{\text{core}}/L_{\text{ext}}$ , where  $L_{\text{core}}$  and  $L_{\text{ext}}$  are the core and extended luminosities, respectively; (10) largest angular size (LAS), measured from the core to the peak in the extended radio structure [following Murphy et al. (1993)] on VLA C array map (if the source was resolved, else measured on VLA A array map) or (combined) ATCA map; and (11) ratio of core luminosity to total X-ray luminosity at 1 keV, the latter  $k$ -corrected with spectral index  $\alpha_x = 1.2$ .

\* observed 4.8 GHz radio properties

that whereas the extended radio powers of DXRBS BL Lacs span a relatively wide range ( $\sim 4$  orders of magnitude), a considerable number of sources (11/44 objects or 25 per cent) have values typical of FR II radio galaxies ( $L_{\text{ext}} > 10^{26}$  W Hz $^{-1}$ ; Owen & Ledlow 1994) and more than half of the sample (25/44 objects or 57 per cent) lies in the regime occupied by both FR Is and FR IIs ( $10^{24.5} < L_{\text{ext}} < 10^{26}$  W Hz $^{-1}$ ; Owen & Ledlow 1994). This means that a *large fraction of the sample are potentially beamed FR IIs*. Regarding only the complete sample the numbers are similar, with 9/31 objects (or 29 per cent) and 18/31 objects (or 58 per cent) having FR II and FR I/II extended radio powers, respectively.

For two and four of the unresolved sources in our sample the calculated upper limits on the extended radio emission fall in the FR II and FR I/II regime, respectively. If these sources have values of the radio core-dominance parameter  $R \gg 1$ , the derived limits might be highly overestimated. In this respect we note that if we use instead the maximum radio core-dominance value observed for the entire sample ( $R \sim 40$ ), the extended radio emission of three of these sources reduces to values typical of FR Is.

In Fig. 9 we have included for comparison also the 1-Jy BL Lac sample (Stickel et al. 1991; Rector & Stocke 2001) (open circles), which to date is the only other sizeable, complete radio flux-limited sample besides the DXRBS. Radio core and extended fluxes at 1.4 GHz are available from high-quality VLA observations for all 37 1-Jy BL Lacs (e.g., Murphy et al. 1993; Cassaro et al. 1999; Rector & Stocke 2001), with the exception of the most southern source (1Jy 2005–489). Three sources, namely, 1Jy 0048–097, 1Jy 0716+714, and 1Jy 2150+173, have featureless optical spectra (Rector & Stocke 2001), and we have used lower limits on the redshifts (see Section 2.2) to calculate luminosities. We note that one source (B2 1147+245) is common to both the 1-Jy and DXRBS BL Lac samples. Fig. 9 shows that the majority in the 1-Jy sample is shifted towards higher extended radio powers relative to the DXRBS. Roughly half the sample (18/37 objects or 49 per cent) has values typical of FR II radio galaxies and more than a third (13/37 objects or 35 per cent) lies in the regime occupied by both FR Is and FR IIs. This shift can be attributed mainly to the different radio flux limits and sky coverages of the two surveys. Both these values are significantly higher for the 1-Jy survey than for the DXRBS (radio flux limits at 5 GHz of 1 Jy and  $\sim 50$  mJy, and sky coverages of  $\sim 10$  and  $< 1$  sr, respectively), thus favoring the selection of high-power sources.

## 4.2 The Radio Morphologies

In the previous subsection we have shown that a large majority ( $\sim 80$  per cent) of the DXRBS BL Lac sample have extended radio powers typical of FR II radio galaxies. Is also their radio morphology consistent with them being relativistically beamed FR IIs? An answer to this question is especially important for that part of the sample with extended radio powers in the overlap regime between FR Is and FR IIs.

The main defining feature of an FR II radio galaxy is the presence of well-collimated jets that terminate in ‘hot spots’, i.e., small areas of high surface brightness. By definition, these hot spots are located towards the ends

of the extended radio lobes (Fanaroff & Riley 1974). However, the radio morphology expected for an FR II viewed at small angles is not entirely clear. The emission from the lobes may overlap in projection giving the appearance of an extended halo. On the near-side a relatively well-collimated, one-sided jet terminating in a hot spot should appear. In some cases we might also expect to see an isolated hot spot on the other side of the amplified jet, due to the (presumed) counterjet. These features are generally observed in steep- and flat-spectrum radio quasars (e.g., Browne et al. 1982; Kollgaard et al. 1990; Murphy et al. 1993; Kapahi et al. 1998; Landt et al. 2006), which are believed to be the relativistically beamed counterparts of FR II radio galaxies. Do we see some or all of them also in the DXRBS BL Lacs?

### 4.2.1 BL Lacs with FR II Extended Radio Powers

Eleven DXRBS BL Lacs have FR II-like extended radio powers ( $L_{\text{ext}} > 10^{26}$  W Hz $^{-1}$ ). Two of these sources, namely, WGA J0043–2638 (Fig. 1d) and WGA J0100–3337 (Fig. 1e), are unresolved on the scales imaged and their association with an FR class remains uncertain. For the remaining nine sources we discuss in the following their radio morphology individually and in decreasing order of the extended radio luminosity.

*WGA J1320+0140.* – The VLA A array map (Fig. 4e) shows the core region to be elongated to the west. Most of the diffuse radio emission is observed perpendicular to the axis of the core elongation and extends to one side only. It has a broad jet-like structure, which appears to be embedded in a lobe. Some low-level extended radio emission is found also along the axis of the core elongation.

*4C +55.17.* – The VLA A array map of Murphy et al. (1993) shows a one-sided jet-like structure and a diffuse extended radio halo to both sides of the core-jet axis. A 408 MHz radio map of similar resolution taken by Browne et al. (1982) shows the one-sided jet to be relatively well-collimated and a potential hot spot can be seen on the other side of the core.

*WGA 1012+06.* – The VLA A array map (Fig. 8c) shows a one-sided jet emanating from the core, which first bends to the south-east and then to the south. A possible hot spot of a counterjet is seen on the opposite side of the core. The core-jet structure appears to be embedded in a diffuse extended radio halo.

*3C 66A.* – The VLA BnA array maps of Ulvestad et al. (1983) show a short (a few arcseconds long) one-sided jet. The core-jet structure is surrounded by a large-scale diffuse radio halo.

*WGA J1231+2848.* – The VLA A array map (Fig. 4b) shows a short ( $\sim 5''$  long) one-sided jet emerging from the core and ending in a hot spot. The combined VLA A+C array map (Fig. 4c) shows that this core-jet structure is embedded in a large-scale diffuse lobe emission. A low-level counterjet seems to be present on the opposite side of the core.

*PMN J0630–24.* – The VLA A array map (Fig. 7d) shows the core region to be elongated to the north. Most of the diffuse radio emission is observed perpendicular to

the axis of the core elongation and extends to one side only. It has a broad jet-like structure. Some low-level extended radio emission is found to the opposite side of the large-scale extended radio structure.

*WGA J1840+5452.* – The VLA A array map (Fig. 5e) shows a short jet-like structure emerging from the core. The jet is observed on the VLA A+C array map (Fig. 5f) to continue over scales of tens of arcseconds, possibly ending in a hot spot.

*WGA J0940+2603.* – The VLA A array map (Fig. 3f) shows two extended lobes to each side of the core that partly overlap. The western lobe contains an embedded broad jet-like structure, whereas the eastern lobe appears to end in a hot spot.

*TEX 0836+182.* – The VLA A array map (Fig. 8a) shows a diffuse jet-like structure emerging from the core and stretching to the south-east. Low-level extended emission on the scales of the jet appears to be present everywhere around the core. The VLA C array map (Fig. 8b) shows a well-collimated jet emerging from the core, which extends to the south-west and therefore almost perpendicular to the jet-like structure seen on smaller scales.

In summary, the radio morphologies of all but two sources are compatible with what is expected for a beamed FR II radio galaxy. In particular, one-sided jets and extended halos surrounding the core-jet structure are observed. Signs of a counterjet are detected in four sources. The radio morphologies of WGA J1320+0140 and PMN J0630–24 are inconclusive. Since these sources are the only ones with elongated cores and have the highest redshifts, radio maps of higher resolution might reveal also in them one-sided jets. The observed broad jet-like structures might then be rather lobes than large-scale diffuse jets.

#### 4.2.2 BL Lacs with FR I/II Extended Radio Powers

In our sample, 25 sources have extended radio powers in the regime where both FR I and FR II radio galaxies are found ( $10^{24.5} < L_{\text{ext}} < 10^{26}$  W Hz<sup>-1</sup>). About a third of these objects (7/25 sources) show a radio morphology expected for a beamed FR II radio galaxy. In the following we describe them individually and in decreasing order of the extended radio luminosity.

*WGA J1744–0517.* – The VLA A array map (Fig. 5a) shows a one-sided jet that emerges from the core and stretches to the north. The core-jet structure is embedded in lobe emission on scales of a few arcseconds.

*WGA J0528–5820.* – The ATCA 6A+6B array map (Fig. 2f) shows two extended lobes to each side of the core. The southern lobe contains an embedded broad jet-like structure, whereas the northern lobe appears to end in a hot spot.

*WGA 1202+44.* – The VLA A array map (Fig. 8d) shows the core to be surrounded by a small ( $\sim 10''$ ) diffuse halo. As the VLA C array map (Fig. 8e) indicates, this halo is most likely the remainder of an extended radio structure that is resolved out on these small scales. The observed large-scale radio emission is indicative of an FR II. Two lobes to each side of the nucleus are visible with the eastern lobe containing a hot spot. The western lobe appears to have an

embedded one-sided jet, but a VLA B array map would be necessary to confirm this.

*B2 1147+245.* – The VLA A array map of Antonucci & Ulvestad (1985) shows a one-sided jet-like structure emerging from the core and extending to the south. A possible hot spot of a counterjet is seen on the opposite side of the core.

*WGA J1936–4719.* – The ATCA 6B array map (Fig. 6b) shows a jet-like structure observed to continue over scales of tens of arcseconds, possibly ending in a hot spot.

*WGA J0245+1047.* – The VLA A array map (Fig. 1f) shows a classical FR II structure, a one-sided jet emerges from the core in direction south-east and a lobe with a hot spot is on each side of the core. However, the VLA A+C array map (Fig. 2a) shows that this source is rather an X-shaped radio galaxy (e.g., Cheung 2007). Large-scale extended lobe emission is visible to both sides of the core and almost orthogonal to the small-scale lobes, thus giving the appearance of an X-shape.

*WGA J1311–0521.* – The VLA C array map (Fig. 4d) shows extended emission on both sides of the core. A lobe with an irregular structure is present on the western side. Since the core appears to be elongated in its direction, this lobe might contain a one-sided jet. A VLA B array map would be necessary to confirm this. The structure on the eastern side of the core is difficult to classify. It might be either a highly irregular lobe with a hot spot or a strongly bended large-scale jet.

Of the remaining 18 sources in this luminosity range, five objects, namely, WGA J0533–4632 (Fig. 3a), WGA J1539–0658 (Fig. 4f), WGA J1834–5948 (Fig. 5d), WGA J1843–7430 (Fig. 6a), and WGA J2330–3724 (Fig. 6e), four of which have been observed with the ATCA, are barely resolved on the scales imaged and their association with an FR class remains uncertain. The other 13 sources are most likely beamed FR I radio galaxies for reasons as follows:

- four sources, namely, EXO 0556–3838 (Fig. 6f), PKS 2316–423 (Fig. 7c), RX J09168+523 (Figs. 7e and 7f), and 1ES 1212+078 (Giroletti et al. 2004), show relatively broad one-sided structures, which seem to be a mixture between a jet and a lobe. This structure is reminiscent of the main characteristic of FR I radio galaxies, which are jets that diffuse already at locations close to the core;

- seven sources, namely, WGA J0032–2849 (Figs. 1a and 1b), WGA J0431+1731 (Fig. 2d), WGA J0449–4349 (Fig. 2e), WGA J1834–5856 (Fig. 5c), WGA J2258–5525 (Fig. 6c), EXO 1811+3143 (Fig. 7a) and ON 325 (Antonucci & Ulvestad 1985), have a core surrounded by a smooth extended, almost circular halo without the embedded one-sided jets typical of FR IIs;

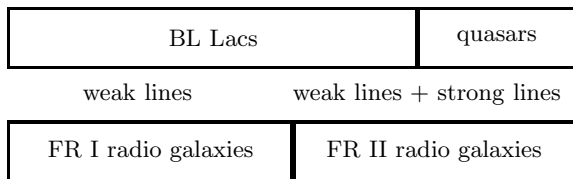
- and finally, the two sources with the lowest extended radio powers and close to the FR I regime, namely, WGA J0428–3805 (Fig. 2c) and WGA J0624–3229 (Fig. 3d), show two well separated radio lobes oriented to the same side of the core and almost perpendicular to each other. This radio morphology is reminiscent of a beamed wide-angle tail (WAT) radio galaxy (e.g., O’Donoghue et al. 1990), which is usually grouped under FR I.

### 4.3 An Inconsistency in the Classification Scheme

We have shown that (*at least*) a third of the DXRBS BL Lacs are beamed FR II radio galaxies. In the following we argue that an heterogeneous parent population for BL Lacs is *expected* given the current classification scheme for radio-loud AGN, which calls for a revision of unified schemes.

Our present classification scheme has a general inconsistency, which is illustrated in the diagram below. We separate radio galaxies and blazars into their subclasses based on different criteria, namely, radio morphology (and so radio power) and emission line strength, respectively. However, observations of *both* beamed and unbeamed sources suggest that these two criteria are not equivalent. Among the radio galaxies, FR Is appear to form a homogeneous class with respect to emission line strength, they have no or only weak emission lines (e.g., Owen et al. 1995; Zirbel & Baum 1995). On the other hand, FR II radio galaxies appear to form a heterogeneous class. Whereas the large majority have strong emission lines, a considerable number of FR IIs exist that have weak emission lines (e.g., Laing et al. 1994; Zirbel & Baum 1995; Tadhunter et al. 1998). Then, since, by definition, BL Lacs are those blazars with weak emission lines, their parent population is *expected* to be heterogeneous. It will contain radio galaxies with no or only weak emission lines, i.e., both FR Is and FR IIs. On the other hand, given that only FR IIs have strong emission lines, the parent population of radio quasars will be homogeneous.

*separation by emission line strength*



*separation by radio power*

Landt et al. (2004) presented a classification scheme for radio-loud AGN that correctly assigns the subclasses within the beamed and unbeamed populations, and we have applied it to the DXRBS BL Lac sample (see Section 2.1 and Table 1, column (3)). Whereas for 9/44 sources their scheme is not applicable, the large majority (32/44 sources or 73 per cent) are classified as weak-lined and only three sources as strong-lined radio-loud AGN. According to the considerations above, the class of strong-lined radio-loud AGN should comprise only FR IIs. Indeed, the three sources in this category, namely, WGA J0245+1047, WGA J1840+5452 and 4C +55.17, have extended radio powers and morphologies consistent with them being beamed FR IIs. Of the nine sources without a classification, three objects, namely, WGA J1320+0140, WGA 1012+06, and 3C 66A, have radio properties compatible with FR IIs and could be strong-lined radio-loud AGN. Candidates for this category are also the sources WGA J0043–2638 and WGA J0100–3337, that have estimated extended radio powers in the FR II regime, but are unresolved on the scales imaged. The remaining four sources without a classification have radio properties compatible with FR Is and are expected to be weak-lined radio-loud AGN.

## 5 FEATURELESS BL LACS

In Section 2.2 we have used the method of Piranomonte et al. (2007) to determine lower limits on the redshifts of eight DXRBS BL Lacs. This method takes into account that the optical spectrum of a BL Lac can appear featureless if it is either at a low redshift ( $z \lesssim 0.6$ ) and strongly beamed or at a high redshift, in which case it can be also moderately beamed. In this section we want to investigate if the observed radio morphologies support this method.

For the majority of featureless DXRBS BL Lacs (5/8 objects) the method of Piranomonte et al. (2007) suggests that they are strongly beamed, whereas three sources, namely, WGA J0940+2603, WGA J1231+2848, and WGA J1539–0658, could be either moderately or strongly beamed. Therefore, we expect the first group to have on average larger values of the radio core-dominance parameter  $R$ , a quantity that is believed to be a suitable beaming indicator, than the second group. Indeed, the first group appears to be on average a factor of  $\sim 2$  stronger core-dominated than the second group ( $\log R = 0.83 \pm 0.35$  and  $0.50 \pm 0.35$ , respectively), but given the small number statistics this result remains suggestive.

It is worth noting that among the first group one source (WGA J0449–4349) is lobe- ( $\log R = -0.33$ ) and not core-dominated as expected by Piranomonte et al. (2007). However, since this source is a high-energy peaked BL Lac (see Section 6), it is possible that its jet emission strongly dominates the host galaxy at optical frequencies, thus rendering the optical spectrum featureless, although it is weak relative to the extended emission at radio frequencies (Giommi et al. 2002). We note also that among the second group one source (WGA J1539–0658) is strongly core-dominated ( $\log R = 1.15$ ), which means that its redshift might be considerably higher than the derived lower limit.

## 6 LOW- AND HIGH-ENERGY PEAKED BL LACS

Depending on their spectral energy distributions (SEDs) BL Lacs are divided into low- (LBL) and high-energy peaked BL Lacs (HBL), i.e., sources with a jet synchrotron emission peak at IR/optical and UV/soft X-ray frequencies, respectively (Padovani & Giommi 1995). So far, two explanations have been proposed for the observed range of SEDs. The oldest hypothesis suggests that BL Lacs have jets with frequency-dependent properties, in particular the higher the frequency, the more isotropic the emission (Maraschi et al. 1986; Ghisellini & Maraschi 1989; Celotti et al. 1993; Georganopoulos & Marscher 1998). Then, a BL Lac appears as an LBL and HBL when viewed at smaller and larger angles, respectively. A competing scenario proposes that BL Lac jets have a wide range of magnetic fields and/or speeds (Giommi & Padovani 1994; Giommi et al. 1995; Padovani & Giommi 1995; Sambruna et al. 1996). The so-called ‘blazar sequence’ builds on this scenario and advocates that the higher the (intrinsic) jet power and the strength of the external, nuclear photon field, the stronger the Compton-cooling of the jet particles, and the lower the synchrotron emission peak frequency (Fossati et al. 1998; Ghisellini et al. 1998).

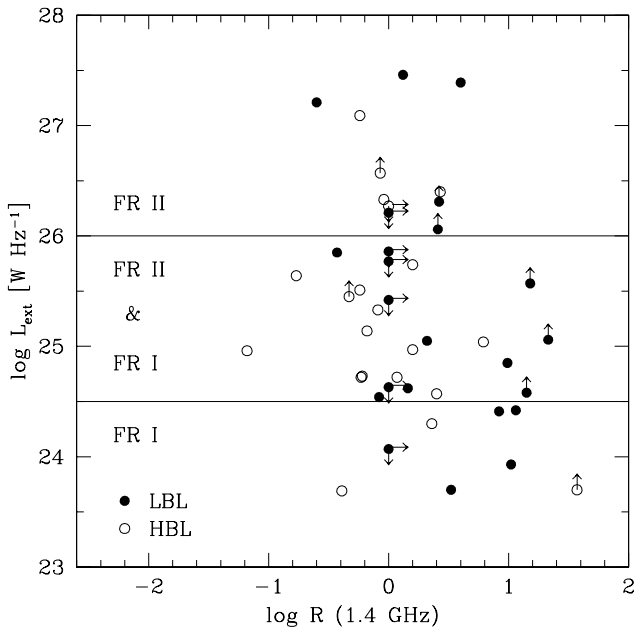


**Figure 10.** As in Fig. 9 for low- (LBL; filled circles) and high-energy peaked BL Lacs (HBL; open circles) from the DXRBS.

The competing explanations for the observed BL Lac SEDs relied mainly on observations of the 1-Jy and EMSS samples. However, given their widely different selection bands (radio and X-ray frequencies, respectively) and (radio) flux limits, these two surveys have most likely presented a strongly biased view. Since the DXRBS contains a sizeable number of both BL Lac subclasses we can now compare for the first time their radio properties relatively free of selection effects.

In Fig. 10 we have plotted the radio core-dominance parameter  $R$  versus the extended radio luminosity at 1.4 GHz for the DXRBS LBL (23 objects, filled circles) and HBL (21 objects, open circles). LBL and HBL have been defined by  $\log L_{\text{core}}/L_x \geq 6$  and  $< 6$ , respectively, where  $L_x$  is the total X-ray luminosity at 1 keV (Padovani & Giommi 1996). Fig. 10 presents in principle a powerful test for both the postulations of the blazar sequence and the two competing scenarios explaining the BL Lac SEDs. The extended radio power is the most suitable measure of *intrinsic* jet power for blazars, and according to the blazar sequence we expect LBL to have on average higher values than HBL. Fig. 10 shows that this is not observed in the DXRBS. Whereas LBL reach a factor of  $\sim 2$  higher extended radio powers than HBL, their average values are very similar ( $\log L_{\text{ext}} = 25.35 \pm 0.23$  and  $25.28 \pm 0.20$  for LBL and HBL, respectively). We note that the quoted averages have been calculated treating both lower and upper limits as detections, but a similar result is obtained, if the limits are omitted. Similar to our approach, Nieppola et al. (2008) have recently pointed out that the blazar sequence might be an artifact of relativistic beaming effects, showing that it is not observed once the powers are corrected for Doppler boosting. However, these authors find for BL Lacs an inverted blazar sequence, which we cannot confirm.

The radio core-dominance parameter  $R$  is believed to

be a suitable indicator of orientation (the higher its value, the smaller the jet inclination angle), and, if orientation determines the SED differences between LBL and HBL, we expect their average values to be different. Fig. 10 shows that LBL have on average a factor of  $\sim 3$  higher radio core-dominance parameters than HBL ( $\log R = 0.53 \pm 0.14$  and  $0.00 \pm 0.13$ , respectively, calculated omitting the limits). This result is similar to what has been found previously for comparisons between LBL from the 1-Jy survey and HBL from the EMSS (e.g., Rector & Stocke 2001) and is usually interpreted in support of the ‘different orientation’ theory for the BL Lac SEDs.

Nevertheless, selection and definition effects can account for this result. Since, by definition, LBL have on average higher radio *core* luminosities (and lower X-ray luminosities) than HBL and in the DXRBS both span a roughly similar range in *extended* radio power (see above), LBL are bound to have higher  $R$  values than HBL. In other words, in a radio-flux limited sample, such as, e.g., the DXRBS, LBL and HBL *are defined* to be those sources with on average higher and lower radio core-dominance parameters, respectively. In order to determine if the relative orientations of the two BL Lac subclasses are indeed different, one needs to use instead an orientation indicator, whose definition is independent of the LBL-HBL one. Such a study was done by Landt et al. (2002), who used the Ca H&K break value (a stellar absorption feature in the optical spectrum) as an orientation indicator, and these authors found no significant differences between LBL and HBL, in support of the claims of Padovani & Giommi (1995).

## 7 SUMMARY AND CONCLUSIONS

Our knowledge of the radio properties of BL Lacs is based mainly on the 1-Jy and EMSS samples. However, these surveys have presented a biased view of BL Lac physics. Therefore, we have obtained deep radio images of a complete sample of 44 BL Lacs selected from the Deep X-ray Radio Blazar Survey (DXRBS). We have observed the northern sources with the VLA in both its A and C configurations and the southern sources with the ATCA in its largest configuration. Our main results can be summarized as follows.

(i) Current unified schemes identify the parent population of BL Lacs with FR I radio galaxies, however, in recent years evidence has accumulated that some BL Lacs might in fact be relativistically beamed FR II radio galaxies. We find that also in the DXRBS, based on both the extended radio powers as well as the radio morphologies, (at least) a third of the BL Lac sample can be identified with relativistically beamed FR IIs.

(ii) We discuss an inconsistency in the current classification scheme for radio-loud AGN, which explains why FR II-BL Lacs are in fact *expected* to exist. This inconsistency emerges since we separate radio galaxies and blazars into their subclasses based on different criteria, namely, radio morphology (and so radio power) and emission line strength, respectively. However, these two criteria are not equivalent.

(iii) The so-called ‘blazar sequence’ posits that the amount of Compton cooling of the jet particles determines the frequency of the synchrotron emission peak (Fossati et al. 1998; Ghisellini et al. 1998). In particular, it

expects low-energy peaked BL Lacs (LBL) to have on average higher *intrinsic* jet powers than high-energy peaked BL Lacs (HBL). We compare the extended radio powers of the DXRBS LBL (23 objects) and HBL (21 objects) and find that, contrary to the expectations of the blazar sequence, their average values are similar ( $\log L_{\text{ext}} = 25.35 \pm 0.23$  and  $25.28 \pm 0.20$ , respectively).

We are currently extending our radio observation program for the DXRBS BL Lac sample to investigate smaller-scale source structure. In a future paper we will present results from VLBI.

## ACKNOWLEDGMENTS

H.L. thanks the astrophysics department of Oxford University for its hospitality during the last months of this work. The VLA is operated by the National Radio Astronomy Observatory, which is a facility of the National Science Foundation operated under cooperative agreement by Associated Universities, Inc. The ATCA is part of the Australia Telescope, which is funded by the Commonwealth of Australia for operation as a National Facility managed by CSIRO.

## REFERENCES

- Antonucci R. R. J., Ulvestad J. S., 1985, *ApJ*, 294, 158  
 Blandford R. D., Payne D. G., 1982, *MNRAS*, 199, 883  
 Browne I. W. A., Orr M. J. L., Davis R. J., Foley A., Muxlow T. W. B., Thomasson P., 1982, *MNRAS*, 198, 673  
 Cassaro P., Stanghellini C., Bondi M., Dallacasa D., Della Ceca R., Zappalà R. A., 1999, *A&AS*, 139, 601  
 Celotti A., Maraschi L., Ghisellini G., Caccianiga A., Maccacaro T., 1993, *ApJ*, 416, 118  
 Cheung C. C., 2007, *AJ*, 133, 2097  
 Fanaroff B. L., Riley J. M., 1974, *MNRAS*, 167, 31  
 Fossati G., Maraschi L., Celotti A., Comastri A., Ghisellini G., 1998, *MNRAS*, 299, 433  
 Georganopoulos M., Marscher A. P., 1998, *ApJ*, 506, 621  
 Ghisellini G., Celotti A., Fossati G., Maraschi L., Comastri A., 1998, *MNRAS*, 301, 451  
 Ghisellini G., Maraschi L., 1989, *ApJ*, 340, 181  
 Giommi P., Ansari S. G., Micol A., 1995, *A&AS*, 109, 267  
 Giommi P., Capalbi M., Fiocchi M., Memola E., Perri M., Piranomonte S., Rebecchi S., Massaro E., 2002, in Giommi P., Massaro E., Palumbo G., eds, *Blazar Astrophysics with BeppoSAX and Other Observatories A catalog of 157 x-ray spectra and 84 spectral energy distributions of blazars observed with BeppoSAX*. ASI/ESA, p. 63  
 Giommi P., Padovani P., 1994, *MNRAS*, 268, L51  
 Giroletti M., Giovannini G., Taylor G. B., Falomo R., 2004, *ApJ*, 613, 752  
 Gregory P. C., Scott W. K., Douglas K., Condon J. J., 1996, *ApJS*, 103, 427  
 Griffith M. R., Wright A. E., 1993, *AJ*, 105, 1666  
 Kapahi V. K., Athreya R. M., Subrahmanya C. R., Baker J. C., Hunstead R. W., McCarthy P. J., van Breugel W., Kollgaard R. I., Wardle J. F. C., Roberts D. H., 1990, *AJ*, 100, 1057  
 Kollgaard R. I., Wardle J. F. C., Roberts D. H., Gabuzda D. C., 1992, *AJ*, 104, 1687  
 Laing R. A., Jenkins C. R., Wall J. V., Unger S. W., 1994, in Bicknell G. V., Dopita M. A., Quinn P. J., eds, *The First Stromlo Symposium: The Physics of Active Galaxies Spectrophotometry of a complete sample of 3CR radio sources: Implications for unified models*. A.S.P., San Francisco, p. 201  
 Landt H., Padovani P., Giommi P., 2002, *MNRAS*, 336, 945  
 Landt H., Padovani P., Perlman E. S., Giommi P., 2004, *MNRAS*, 351, 83  
 Landt H., Padovani P., Perlman E. S., Giommi P., Bignall H., Tzioumis A., 2001, *MNRAS*, 323, 757  
 Landt H., Perlman E. S., Padovani P., 2006, *ApJ*, 637, 183  
 Maraschi L., Ghisellini G., Tanzi E. G., Treves A., 1986, *ApJ*, 310, 325  
 Maraschi L., Tavecchio F., 2003, *ApJ*, 593, 667  
 Marchã M. J. M., Browne I. W. A., Impey C. D., Smith P. S., 1996, *MNRAS*, 281, 425  
 Morris S. L., Stocke J. T., Gioia I. M., Schild R. E., Wolter A., Maccacaro T., Della Ceca R., 1991, *ApJ*, 380, 49  
 Murphy D. W., Browne I. W. A., Perley R. A., 1993, *MNRAS*, 264, 298  
 Nieppola E., Valtaoja E., Tornikoski M., Hovatta T., Kotiranta M., 2008, *Blazar Sequence - An Artifact of Doppler Boosting*, astro-ph/0803.0654  
 O'Donoghue A. A., Eilek J. A., Owen F. N., 1990, *ApJS*, 72, 75  
 Owen F. N., Ledlow M. J., 1994, in Bicknell G. V., Dopita M. A., Quinn P. J., eds, *The First Stromlo Symposium: The Physics of Active Galaxies The FR I/II break and the bivariate luminosity function in Abell clusters of galaxies*. A.S.P., San Francisco, p. 319  
 Owen F. N., Ledlow M. J., Keel W. C., 1995, *AJ*, 109, 14  
 Padovani P., 2007, in *The Multi-Messenger Approach to High-Energy Gamma-Ray Sources Vol. 309, The blazar sequence: Validity and predictions*. Astrophysics and Space Science, p. 63  
 Padovani P., Giommi P., 1995, *ApJ*, 444, 567  
 Padovani P., Giommi P., 1996, *MNRAS*, 279, 526  
 Padovani P., Giommi P., Landt H., Perlman E. S., 2007, *ApJ*, 662, 182  
 Perlman E. S., Padovani P., Giommi P., Sambruna R., Jones L. R., Tzioumis A., Reynolds J., 1998, *AJ*, 115, 1253  
 Perlman E. S., Stocke J. T., 1993, *ApJ*, 406, 430  
 Piranomonte S., Perri M., Giommi P., Landt H., Padovani P., 2007, *A&A*, 470, 787  
 Rawlings S., Saunders R., 1991, *Nature*, 349, 138  
 Rector T. A., Stocke J. T., 2001, *AJ*, 122, 565  
 Rector T. A., Stocke J. T., Perlman E. S., Morris S. L., Gioia I. M., 2000, *AJ*, 120, 1626  
 Sambruna R. M., Maraschi L., Urry C. M., 1996, *ApJ*, 463, 444  
 Stickel M., Padovani P., Urry C. M., Fried J. W., Kühr H., 1991, *ApJ*, 374, 431  
 Stocke J. T., Morris S. L., Gioia I. M., Maccacaro T., Schild R., Wolter A., Fleming T. A., Henry J. P., 1991, *ApJS*, 76, 813

- Strittmatter P. A., Serkowski K., Carswell R., Stein W. A.,  
Merrill K. M., Burbidge E. M., 1972, ApJ, 175, L7
- Tadhunter C. N., Morganti R., Robinson A., Dickson R.,  
Villar-Martin M., Fosbury R. A. E., 1998, MNRAS, 298,  
1035
- Ulvestad J. S., Johnston K. J., Weiler K. W., 1983, ApJ,  
266, 18
- Urry C. M., Padovani P., 1995, PASP, 107, 803
- Urry C. M., Padovani P., Stickel M., 1991, ApJ, 382, 501
- Urry C. M., Scarpa R., O'Dowd M., Falomo R., Pesce J. E.,  
Treves A., 2000, ApJ, 532, 816
- White N. E., Giommi P., Angelini L., , 1995,  
<http://wgacat.gsfc.nasa.gov/wgacat/wgacat.html>
- White R. L., Becker R. H., 1992, ApJS, 79, 331
- Zirbel E. L., Baum S. A., 1995, ApJ, 448, 521

This paper has been typeset from a  $\text{\TeX}/\text{\LaTeX}$  file prepared  
by the author.